Λ Polarization in Heavy Ion Collisions

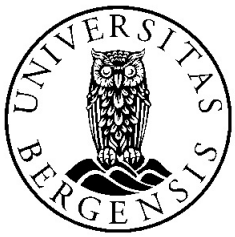

Master Thesis in

High Energy Physics and Theoretical Physics

by

Robert C. Glastad

Department of Physics and Technology

University of Bergen

June, 2015

Abstract

The initial angular momentum of the system formed in peripheral heavy ion collisions is of order $10^6\hbar$. This leads to strong momentum space anisotropies, evident in the directed, and elliptic flow. In the almost perfect fluid formed in the central reaction zone, shear flow may facilitate the onset of a Kelvin-Helmholtz instability, which may enhance rotation. The large local angular momentum is thought to lead to a large global transverse polarization due to spin-orbital-momentum coupling in QCD. The STAR collaboration at RHIC recently measured $|P_{\Lambda,\overline{\Lambda}}|$ to no more than 2%. Polarization was averaged over large centralities and the azimuth of the Λ momentum. The polarization is predicted to be 9% if the Λ has momentum in the reaction plane. Presented here are analytic, non-relativistic results for Λ transverse polarization in $\sqrt{s_{NN}} = 2.76A{\cdot}\text{TeV}$, $b = 0.7b_{Max}$ collisions using an exact, rotating hydrodynamical model with a modified spin-1/2 Cooper-Frye freeze-out. The Λ polarization is predicted to become large for increasing center of mass transverse momenta in the reaction plane; little y-dependence is displayed. The polarization is 1% for vanishing center of mass transverse momentum; it increases to 16% for $p_x = \pm 4$ for any choice in p_y. The polarization points in the negative y-direction. For the first time, the radial and axial components of polarization were calculated.

Acknowledgements

First of all, I would like to extend my thanks to the University of Bergen, which gave me an extra day to make this document more viable for print – and avoid drastically lowering my grade.

Next, I would like to thank professor Laszlo Csernai, who has been my advisor over these couple of years. Although we did not get to work much together, I value the time we had. I admire his proficiency and level of knowledge, and I regret not having gotten the most out of my time with him. I also enjoyed working with Yilong Xie, who has done a great job with our code, as I had trouble compiling it. Thanks to Stephen Wolfram and the Wolfram team for Mathematica; also Eben Upton and his collaborators for the Raspberry Pi; the open source community, in general, has been of incredible help over these last years. Thank you all!

I would also like to thank my fellow students, the professors, doctoral candidates, and all the people who work at the Department of Physics and Technology. Particular thanks to Inspector Villy, who greats me with the same level of enthusiasm and friendliness every single time I see him.

Particular thanks also to those of us who survived together, Kristoffer, Torstein, Lars, Andre (I can't write that damn accute accent!), Jorgen (nor your thing), Haakon(!), Truls, and Kristian. I cannot believe not *one* of us has yet died of cancer. At least we have tested rather rigorously the hypothesis that the Universe conforms to our negative vibes. That is something I add to this thesis; hopefully it will bump my grade somewhat.

And, lastly, special thanks to Eirik and Hans for all the interesting topics, discussions, and thoughts over the years. And, of course, my family for keeping

up with me even though I have been frustrated at times. My girlfriend, Heidi, who sometimes has to listen to my rants and who has been the most wonderful support to me.

Contents

Chapter 1

Preliminaries

This is a master's thesis in theoretical and high energy physics accompanied by a paper made under the guidance of professor László Csernai. I was fortunate to work with him on a problem pertaining to his work in relativistic heavy ion collisions. I also had the pleasure of working with Yilong Xie. The paper is a small contribution to the field of high-energy and nuclear physics.

The novel feature of this work [**1**] is the use of a recently proposed exact analytical, self-similar rotating hydrodynamics model combined with a Cooper-Frye freeze-out formulated to accommodate spin-1/2 particles to calculate the Λ polarization in peripheral heavy ion collisions. Frankly, our discovery that the terms in the polarization integral hitherto neglected were quite significant is indeed the novel feature. Small as it may seem, I am under the impression that it was a suprise to those working in the field, so I consider the work well done. **I use natural units, $\hbar = c = k_B = 1$, in what follows.**

1.1 Special Relativity

Invariant quantities play a central role in heavy ion collisions, and allow us to express the mathematics in a fashion that is frame-independent. Let m be the mass of a particle. We denote its position by

$$x^\mu = (t, \boldsymbol{x}), \tag{1.1}$$

and its momentum by

$$p^\mu = (E, \boldsymbol{p}), \tag{1.2}$$

where t is time, $\boldsymbol{x}$ is the position vector, E is the particle energy

$$E = \sqrt{\boldsymbol{p}^2 + m^2}; \tag{1.3}$$

$\boldsymbol{p}$ is three-momentum. The inner product of any two four-vectors is invariant (in general, the contraction of all indices is invariant):

$$p^2 = m^2 = E^2 - \boldsymbol{p}^2. \tag{1.4}$$

We transform using the Minkowski metric,

$$\begin{pmatrix} 1 & 0 & 0 & 0 \\ 0 & -1 & 0 & 0 \\ 0 & 0 & -1 & 0 \\ 0 & 0 & 0 & -1 \end{pmatrix}. \tag{1.5}$$

For example, $x_\mu = g_{\mu\nu} x^\nu$. Since invariance is the name of the game, rapidity is a convenient way to characterize speeds in. Let

$$(E, p_x, p_y, p_z) \to (E, \boldsymbol{p}_T, y), \tag{1.6}$$

and define

$$y = \tanh^{-1} \frac{p_z}{E} = \frac{1}{2} \ln \left(\frac{E + p_z}{E - p_z} \right). \tag{1.7}$$

We do this since all directions perpendicular to the direction of motion are left unchanged; a vector in the transverse plane does not change its length or direction when transforming from one frame to the other. Furthermore, for one-dimensional boosts, rapidities are conveniently added. An invariant related to this is the transverse mass,

$$m_T = \sqrt{m^2 + p_T^2}. \tag{1.8}$$

Remember there is an implicit dependence on the polar angle θ in p_z; for ultra-relativistic particles, this leads to the definition of pseudorapidity ($m << |\boldsymbol{p}|$)

$$\eta = \frac{1}{2}\ln\frac{1+\cos\theta}{1-\cos\theta} = \ln\left(\cot\frac{\theta}{2}\right). \tag{1.9}$$

In frequent use is the (3+1)D coordinate system $(\boldsymbol{x}_T, y, \tau)$ to describe fluid flow in relativistic fluid dynamics. Here $\tau = \sqrt{t^2 - z^2}$ is proper time. Collisions take place at small values of z, whereas large rapidities often are assumed to be ∞ (corresponding to $v \to c$. This corresponds to small values of rapidity, commonly referred to as mid-rapidity; boost invariant boundary conditions often mean we treat the system in the mid-rapidity region.

The invariant cross section is

$$\sigma_{inv} = E\frac{d^3\sigma}{dp^3}, \tag{1.10}$$

which may be manipulated to suit the situation. For example, if the system is cylindrically isotropic, we have (partially integrated)

$$dp^2 = 2\pi p_T dp_T dp_z, \tag{1.11}$$

which, with $dp_z/E = dy$, yields

$$\sigma_{inv} = \frac{d^2\sigma}{2\pi p_T dp_T dy}. \tag{1.12}$$

1.2 Statistical Mechanics, Quantum Mechanics and Observables

In classical statistical mechanics, phase space refers to the union of configuration space with its cotangent space. The trajectory (x_i, p_i) uniquely determines the system's microstate for a given Hamiltonian, H. Kinetic theory is then reduced to the art of counting the number of microstates, and finding the most likely macrostate. This corresponds to an equilibrium state, or the state with maximum entropy. The coordinates are related via Hamilton's equations of motion

$$\dot{x}_i = \frac{\partial H}{\partial p_i} \tag{1.13}$$

$$\dot{p}_i = -\frac{\partial H}{\partial x_i}, \tag{1.14}$$

and any observable has equation of motion

$$\dot{O} = \frac{\partial O}{\partial t} + \{A, H\}, \tag{1.15}$$

where $\{O, H\}$ is the Poisson bracket.

In quantum mechanics, however, we have only the wavefunction as a function of the positions, momenta and other properties, like spins, of the particles in the system, $|\Psi\rangle$. The wave function lives in Fook space, the union of all Hilbert spaces associated with the system. The wave equation satisfies Schrödinger's equation

$$i\,|\dot{\Psi}\rangle = H\,|\Psi\rangle\,. \tag{1.16}$$

If there are no external forces acting on the system, we separate the time-dependence from the energy dependence:

$$i\,|\dot{\Psi}\rangle = e^{-iEt}E\,|\Psi_E\rangle\,. \tag{1.17}$$

The hat denoting the fact that the Hamiltonian, or any observable, is an operator has been omitted. Let $|\psi_i\rangle$ denote a complete set of energy eigenvectors in Fook space, then

$$H\,|\psi_i\rangle = E_i\,|\psi_i\rangle\,. \tag{1.18}$$

This eigenvector corresponds to the eigenvalue E_i, which is the energy associated with the state; this is the energy one would measure if the system was found in the state $|\psi_i\rangle$. We will stick to a general basis of operator eigenvalues, each of which allows for the complete knowledge of the system within the confines of the commutation relations. In a complete basis of orthonormal kets $\{|\psi_i\rangle\}$ any state can be expressed as

$$|\Psi\rangle = \sum_i c_i\,|\psi_i\rangle\,, \tag{1.19}$$

with $\langle\psi_i|\psi_j\rangle = \delta_{ij}$. The density operator in this set is given by

$$\rho = \sum_i c_i\,|\psi_i\rangle\,\langle\psi_i|\,. \tag{1.20}$$

Its action on the general state $|\Psi'\rangle$,

$$\rho \left|\Psi'\right\rangle = \sum_i c_i \left|\psi_i\right\rangle \left\langle\psi_i\right| \left[\sum_j c_j \left|\psi'_j\right\rangle\right\rangle = c_j^2, \tag{1.21}$$

denotes the probability of finding the particle whose wave function is $|\Psi'\rangle$ inhabiting the pure state $|\psi'_j\rangle$. Any observable is weighted by this transition probability, so we have the relation

$$\langle O\rangle = \mathrm{tr}(\rho O), \tag{1.22}$$

where ρ is the projection operator

$$\rho = \sum_i \left|\psi_i\right\rangle \left\langle\psi_i\right|. \tag{1.23}$$

We use von Neumann's equation of motion for the Schrödinger picture (where $\dot{\rho}_i = 0$)

$$i\frac{d}{dt}\rho = [H, \rho], \tag{1.24}$$

or Heisenberg's in Heisenberg's picture (with $\dot{\rho} = 0$)

$$i\frac{d}{dt}O_H = \frac{\partial O}{\partial t} + i[O, H] \tag{1.25}$$

Wigner's 1931 theorem, that there is a one-to-one correspondence between observables and the ray space defining the pure states (and hence *all* states), has proved an important result for theoretical physics. The ray space is defined as

$$\mathcal{R} = \{\rho(|\psi\rangle) = \left|\psi\right\rangle \left\langle\psi\right|, \text{ such that } |\psi\rangle \in \mathcal{B}\}, \tag{1.26}$$

where $\mathcal{B}$ is the unit ball,

$$\mathcal{B} = \{|\psi\rangle \in \mathcal{H}, \text{ such that } \langle\psi|\psi\rangle = 1\}. \tag{1.27}$$

Exploiting this fact, we can consider any transformation we like, provided it can be made coherent. Hilbert space is a gauge invariant space due to the fact that a local phase transformation preserves probabilities, i.e., if $|\Psi\rangle \to |\Psi'\rangle = e^{\alpha(x)}|\Psi\rangle$, then

$$\langle\Psi'|\Psi'\rangle = \left\langle\Psi|\Psi\right\rangle. \tag{1.28}$$

Wigner's theorem was foundational to the advent of internal symmetries as suggested by Yang and Mills, which came to dominate theoretical particle physics. They considered the choosing isotopic spin gauge as defining a preferential direction in space. This was not without problems though, since it introduced 12 independent field components countering the variation in the Lagrangian density. And the bosons were massive! Not many years later this led to Higgs' postulate, that there would exist a field that broke the symmetries of Gell-Mann's highest level of symmetry, giving rise to the massive gauge bosons in the weak interaction.

In heavy ion physics, we use the Wigner transformation to relate classical observables to the matrix elements of ρO, here in configuration space representation

$$\langle O(x,p)\rangle = \frac{1}{(2\pi)^4}\int d^4y e^{-ipy}\,\langle x-y/2|O|x+y/2\rangle\,. \tag{1.29}$$

These are what are referred to as *quasiprobability* distributions. Wigner's theorem associates to each observable a phasespace distribution function corresponding to the observable, defined via the relation between statistical ensembles and observables,

$$< O >= Tr(\hat{\rho}\hat{O}). \tag{1.30}$$

This function is not non-negative, however, which may be a problem, but it seems negative probabilites are extricably linked to uncertainty. We use the single-particle Fermi-Jüttner distribution

$$f(x,p) = \frac{1}{e^{(p^\mu u_\mu - \mu(x))/T(x)}+1}, \tag{1.31}$$

where p is four-momentum, u is four-flow and $\mu(x)$ the chemical potential. The temperature is $T(x)$.

For a hydrodynamical context, in particular, we have the situation where the energy-momentum tensor is a quantum mechanical operator,

$$T^{\mu\nu} = \mathrm{tr}(\hat{\rho} : \hat{T}^{\mu\nu} :), \tag{1.32}$$

where $\hat{T}^{\mu\nu}$ is composed of the fields, and normal ordering implies one arranges annihilation operators to the right of all creation operators. We want to find the phasespace distribution function associated with this given the particular

Lagrangian density. Strictly speaking, $T^{\mu\nu}$ comes about by considering an infinitesimal boost and rotation invariance in spacetime.

1.2.1 Polarization of a Free Electron

An example of using these relations follows as we analyze the polarization of a free electron, described by

$$|p,s\rangle = c_+ |p,1/2\rangle + c_- |p,-1/2\rangle \,, \tag{1.33}$$

where

$$|p,s\rangle (x) = f(x,p)\chi_s, \tag{1.34}$$

and $\chi_{1/2} = \begin{pmatrix} 1 \\ 0 \end{pmatrix}$ and $\chi_{-1/2} = \begin{pmatrix} 0 \\ 1 \end{pmatrix}$ are its spin projections; $f(x,p)$ the spatial part of the wavefunction. The electron is said to be right-handed polarized (or has a helicity of $+1$) if $c_+ = 1$ and $c_- = 0$. Let $\boldsymbol{P}$ denote the spatial polarization vector. Then

$$\boldsymbol{P} = \langle p,s|\boldsymbol{\sigma}|p,s\rangle = \begin{pmatrix} c_+^* c_- + c_+ c_+^* \\ i(c_+ c_-^* - c_+^* c_-) \\ c_+^* c_- - c_+ c_-^* \end{pmatrix}, \tag{1.35}$$

where $\boldsymbol{\sigma} = (\sigma_1, \sigma_2, \sigma_3)$ are the Pauli matrices. Since $|c_+|^2 + |c_-|^2 = 1$, the electron is maximally polarized. But that is *one* electron. In experiments, we use mostly unpolarized beams, and thus have a statistical ensemble of particles with a given polarization. So we must find the probability distribution prior to finding the observed polarization, via

$$\langle \boldsymbol{P} \rangle = C_+ \langle p,1/2|\boldsymbol{\sigma}|p,1/2\rangle + C_- \langle p,-1/2|\boldsymbol{\sigma}|p,-1/2\rangle \,, \tag{1.36}$$

where $C_\pm$ refer to the observed probability for either state. For $C_\pm = \frac{1}{2}$ the beam is completely unpolarized.

The polarization of Λ's in particle physics is often measured using the angular distribution of decay proton in the Λ frame of reference. Having performed a measurement to distinguish the number of particles with spin up (down) you attain a cross section for spin up (down). The polarization of hyperons is then given by the following ratio:

$$P_\Lambda = \frac{\sigma_+ - \sigma_-}{\sigma_+ + \sigma_-}. \tag{1.37}$$

As we saw with the electron, this is a number between $+1$ and -1, where 0 corresponds to unpolarized, and $+(-)$ 1 refers to completely polarized spin up (down).

1.2.2 Why Glauber states?

A Glauber state is a minimally uncertain coherent state $|\alpha\rangle$, which is an eigenvector of annihilation operator, a, i.e.,

$$a\,|\alpha\rangle = \alpha\,|\alpha\rangle\,, \qquad \langle\alpha|\alpha\rangle = 1. \tag{1.38}$$

These states form the basis for the initial conditions for many hydrodynamic models. Since the eigenvectors of the operators on their respective Hilbert spaces form a complete basis for the Fook space, any state may be expanded in any of of the complete bases of Fook space. Expanded in the number representation $\{|n\rangle\}$,

$$|\alpha\rangle = \sum_{n=0}^{\infty} c_n\,|n\rangle\,, \tag{1.39}$$

Operating on this with the annihilation operator, we get

$$a\sum_{n=0}^{\infty} c_n\,|n\rangle = \sum_{n=0}^{\infty} c_n\sqrt{n}\,|n-1\rangle\,. \tag{1.40}$$

Since $|\alpha\rangle$ is an eigenvector of a,

$$\sum_{n=0}^{\infty} c_n\sqrt{n}\,|n-1\rangle = \alpha\sum_{n=0}^{\infty} c_n\,|n\rangle\,. \tag{1.41}$$

Multiplying from the left by $\langle m|$, we get

$$\langle m|\sum_{n=0}^{\infty} c_n\sqrt{n}\,|n-1\rangle = c_{m+1}\sqrt{m+1} = \alpha c_m, \tag{1.42}$$

which, by induction,

$$c_n = \frac{\alpha^n}{\sqrt{n!}}c_0, \tag{1.43}$$

and, thus,

$$|\alpha\rangle = c_0 \sum \frac{\alpha^n}{\sqrt{n!}} |n\rangle \,. \tag{1.44}$$

We have

$$\begin{aligned} 1 =& |c_0|^2 \sum_{n,m=0} \frac{(\alpha^*)^m \alpha^n}{\sqrt{nm}} \langle m|n\rangle \\ =& |c_0|^2 \sum_n \frac{|\alpha|^{2n}}{n} \\ =& |c_0|^2 e^{-|\alpha|^2}, \end{aligned}$$

so $c_0 = e^{-|\alpha|^2/2}$, or

$$|\alpha\rangle = e^{-|\alpha|^2/2} \sum_{n=0}^{\infty} \frac{\alpha^n}{\sqrt{n!}} |n\rangle \,. \tag{1.45}$$

Glauber states make ideal initial states for hydrodynamics calculations due to the fact that

$$\langle x\rangle = (1/\sqrt{2}\lambda) \langle\alpha|a + a^*|\alpha\rangle = (1/\sqrt{2}\lambda)(\alpha + \alpha^*), \tag{1.46}$$

and

$$\langle k\rangle = (\lambda/\sqrt{2}i) \langle\alpha|a - a^*|\alpha\rangle = (\lambda/\sqrt{2}i)(\alpha - \alpha^*), \tag{1.47}$$

with $\langle\alpha| a^* = \alpha^* \langle\alpha|$ and $a|\alpha\rangle = \alpha|\alpha\rangle$, and a variance

$$\begin{aligned} \langle x^2\rangle =& (1/2\lambda^2) \langle\alpha| : (a + a^*)^2 : |\alpha\rangle \\ =& (1/2\lambda^2) \langle\alpha|(aa + 2a^*a + (a^*)^2)|\alpha\rangle \\ =& (1/2\lambda^2)((\alpha + \alpha^*)^2 + 1), \end{aligned}$$

and similarly

$$\begin{aligned}\langle k^2\rangle &= -(\lambda^2/2)\langle\alpha| : (a-a^*)^2 : |\alpha\rangle \\ &= -(\lambda^2/2)\langle\alpha| : a^2 - aa^* - a^*a + (a^*)^2 : |\alpha\rangle \\ &= -(\lambda^2/2)\langle\alpha|a^2 - 2a^*a + (a^*)2 - 1|\alpha\rangle \\ &= -\lambda^2/2((\alpha-\alpha^*)^2 - 1),\end{aligned}$$

having used $aa^* = 1 + a^*a$ from the commutation relation in the process of normal ordering. The large interest in terms of initial states in heavy ion collisions is evident from the uncertainty relation

$$\sqrt{\langle x^2\rangle - \langle x\rangle^2}\sqrt{\langle k^2\rangle - \langle k\rangle^2} = \frac{1}{2}. \tag{1.48}$$

These states are also referred to as displaced ground states. A similar analysis holds for other complementary coordinates, i.e., those obeying a commutation (anti-commutation) relation.

1.3 Hydrodynamics

Continuum mechanics is the field which governs relativistic fluid dynamics. We describe the bulk properties of matter as if they were continuous, and define fluid particles whose properties are related to microscopic properties through statistical ensembles (like pressure being millions of collisions perpendicular to a boundary). The bulk properties of the fluid as a whole are then similar to that of the fluid particles, whose bulk properties are governed by constituent relations and boundary conditions.

This allows us to make general statement about the conservation of energy and momentum, and possibly conserved charges.

$$\partial_\nu T^{\mu\nu} = 0, \tag{1.49}$$

and

$$\partial_\mu n_i u^\mu, \tag{1.50}$$

To every fluid particle, we assign a timelike four-vector

$$u^\mu = \frac{dx^\mu}{d\tau} = (\gamma, \gamma\boldsymbol{v}), \tag{1.51}$$

everywhere tangent to the fluid wordline. The operator

$$\Delta^{\mu\nu} = g^{\mu\nu} - u^\mu u^\nu \tag{1.52}$$

yields the spatial vector associated with a vector, or the shear/pressure on some surface in spacetime associated with a tensor.

Given the phase space density $f(x,p)$ the local particle density and particle flow are

$$n = \int d^3p f(x,p), \tag{1.53}$$

$$\boldsymbol{j} = \int \boldsymbol{v} f(x,p), \tag{1.54}$$

respectively. Together they yield a particle four-current

$$N^\mu = \int \frac{d^3p}{p^0} p^\mu f(x,p). \tag{1.55}$$

For energy and momentum density flow, we need a tensor of rank 2, which we denote $T^{\mu\nu}$. The energy density and energy flow are T^{00} and T^{i0}, respectively, while the momentum (density) and momentum current are given by T^{0i} and T^{ik}, respectively. Together they give

$$T^{\mu\nu} = \int \frac{d^3p}{p^0} p^\mu p^\nu f(x,p). \tag{1.56}$$

Specifying $f(x,p)$ requires a detailed analysis of a given problem.

A fluid satisfying the Euler equation

$$(\partial_t + \boldsymbol{v}\nabla)\boldsymbol{v} = \frac{-\nabla P}{nm}, \tag{1.57}$$

is called a perfect fluid. It is non-viscous and void of energy dissipation. These equations together with an EoS close the system of equations, allowing for at least attempt at solving. A frequently used EoS is

$$\epsilon = \kappa P = \kappa n T, \tag{1.58}$$

where $\kappa = 1/v_s^2$, the compressibility, is inverse to the square of the velocity of sound, n is the number density, and T the temperature.

We need to entertain the idea that collisions may take place,and we achieve

some handle on it by assuming *molecular chaos* applies, and that the probability for a collisions is proportional to the product of the phasespace densities of the two single-particle distribution functions. If the particles are in momentum states p, p_1 before the collisions, and p', p_1' after, then the Boltzmann transport equation reads

$$p^\mu \partial_\mu f(x,p) = \frac{1}{2}\int \frac{d^3p_1}{p_1^0}\frac{d^3p_1'}{p_1'^0}\frac{d^3p'}{p'^0} \times \left[f(x,p')f(x,p_1')W(p',p_1'|p,p_1) - f(x,p)f(x,p_1)W(p,p_1|p',p_1')\right].$$

It is important to mention that these formulae do not apply in non-equilibrium situations with strong coupling between constituents; for those there are cascade models and other fluid dynamical schemes one would employ. As we will see, viscous corrections to ideal, inviscid hydrodynamics are becoming increasingly important in heavy ion collisions.

At some point during the evolution of the fireball, the energy density is such that the quarks and gluons recombine to make hadrons. This chemical freeze-out takes place at $T \approx 150$ MeV. After the chemical freeze-out, the hydrodynamical evolution continues until a given condition is met. Conditions may also be crosschecked. Often this is a given FO temperature, or a energy density. The point is that the mean distance between fluid particles is so large that they have stopped interacting. At points in spacetime where the conditions are met, we select a spacetime surface Σ, and start counting the particles using the Cooper-Frye FO

$$E\frac{dN}{dp^3} = \int_\Sigma g(s)\Sigma_\mu p^\mu f(x,p), \tag{1.59}$$

where $g(s) = (2s+1)$ is the number of spin states. The FO surface is chosen such that $[T^{\mu\nu}d\Sigma_\nu] = 0$, $[N^\mu d\Sigma_\mu] = 0$, and $dS \geq 0$. To determine the FO temperature normally one employs p_T spectra for hadrons. During all stages, advanced interferometry reveals the system size, angular velocity, and particle correlations, probing the general properties of the system. They may also be necessary simply to detect rotation, as is done in the case of astrophysics, or in relativistic heavy ion collisions in which a strong antiflow may cancel the strong directed flow building up with increasing energies. Particle correlations refer to particles in symmetric or anti-symmetric particle configurations in Hilbert space, where all the spooky action at a distance takes place.

1.3.1 Thermodynamical Relations

We use several thermodynamical relations, most notably the number density (baryon number), n. However, irrespectively of an equation of state, we may use the laws of thermodynamics. The first states

$$\epsilon = \sigma T - P + \mu n, \tag{1.60}$$

where ϵ is the energy density σ the entropy density and n the number density; μ, P, and T are chemical potential, pressure, and temperature, respectively.

If we differentiate this, we get

$$d\epsilon = \mu dn + T d\sigma, \tag{1.61}$$

and

$$dP = n d\mu + \sigma dT, \tag{1.62}$$

using the Gibbs-Duhem relation.

Entropy density is added to the hydrodynamical equations listed above as

$$\partial_t \sigma + \nabla(\sigma \boldsymbol{v}) = 0 \tag{1.63}$$

1.3.2 Scaling variables

Scaling is simply choosing axes and varibles such that they make your life a bit easier. It is closely related to the comoving derivative. In our model, we use temperature and density profiles assumed to be time-independent with respect to the scaling variable, s,

$$s = \frac{x^2}{X^2} + \frac{y^2}{Y^2} + \frac{z^2}{Z^2}, \tag{1.64}$$

where (x, y, z) is the position of a fluid particle in the matter which extends to (X, Y, Z). We have a cylindrically symmetric fireball, so we perform the transformation

$$(x, y, z) \to (r, \phi, y), \tag{1.65}$$

where $r^2 = x^2 + z^2$, $\phi = \tan^{-1}(z/x)$, and $y = y$. Furthermore, we define the $R = R_{\text{out}}$, $S = R_{\text{side}}$, and $Y = R_{\text{long}}$ by substituting $\phi \to r\phi$, so that all

dimensions are the same.

Scaling is now introduced via

$$\begin{aligned} s_r =& r^2/R^2 \\ s_\phi =& (r\phi)^2/S^2 \\ s_y =& y^2/Y^2, \end{aligned}$$

where S is the displacement along the outer surface of the fluid ($S_0 = 0$ for $\phi_0 = 0$; $S = R\phi$). Since we have a cylindrically symmetric fireball, there cannot be any dependence on ϕ in the number density our temperature profile. Thus, we introduce the scaling variable

$$s = s_r + s_y = \frac{r^2}{R^2} + \frac{y^2}{Y^2}. \tag{1.66}$$

We know these facts because

$$(\partial_t + \boldsymbol{v}\nabla)s_r = (\partial_t + \boldsymbol{v}\nabla)s_y = 0. \tag{1.67}$$

Chapter 2

Introduction

We probe Quantum Chromodynamics (QCD) under extreme conditions in relativistic heavy ion collisions. First of all: We assume the system may be treated hydrodynamically; i.e., there is some degree of statistical homogeneity. Fermi suggested chemical equilibrium would be achieved due to the large energy density in a small spacetime region. Landau then proposed that, though chemical equilibrium would not be established immediately, thermal equilbrium is achieved rapidly [**2**]. Hwa gave the interpretation of a hadronic gas with an uncountable number of degrees of freedom due to a large number of fermionic degrees of freedom within the hadrons [**3**]. Bjorken introduced the idea of boost invariant boundary conditions for the mid-rapidity region [**4**]. A number of exact [**5**, **6**, **7**] and numerical solutions [**8**, **9**] to both equilibrium and non-equilibrum fluid dynamics have been established through, among others, the work of Israel and Stewart [**10**]. These hypotheses have proven enormously successful in predicting a number of things: nuclear stopping, the plateu in multiplicity per unit rapidity in the mid-rapidity region, large directed and elliptic flow in peripheral collisions. Today, there is an enormous interest in finding the specific viscosity of the dense and hot matter created in heavy ion reactions. It is a measure of how the fluid in question accommodates collective motion within it. If η/s is large, the fluid will transfer the kinetic energy of constituents into internal energy more easily. There would be no flow components if the matter had had a large specific viscosity. The low ratio η/s permits large fluctuations in the hot and dense matter. As energies increase, so to do fluctuations, and they are now bigger than the v_1 flow in peripheral heavy ion collisions. It should be noted, however, that the v_1 has diminished as energies increase.

2.1 General Interest in Heavy Ion Collisions

The large interest in heavy ion collisions is dual: First, there is the exploration of the phase diagram of QCD. Unique to QCD is that it is non-Abelian. The gauge bosons themselves carry charge, and may emit gluons to change their color in addition to interactions with quarks. This leads to a notoriously difficult formalism in which to compute the action of the field. The phase diagram has been established using perturbative Quantum ChromoDynamics (pQCD) in regions where strong force is rather weak. This is the phenomena of confinement. As quarks are separated, more and more energy is required to pull them further apart, and eventually the potential energy in the field is sufficient to produce the required quark-anti-quark so that the quarks remain confined. At small distances (large energies/densities), however, deconfinement takes place.

Second, there are still hopes some odd signal will appear in one or the other detector, to pave way for the advent of new physics. Non-perturbative QCD is a mathematically intractable problem, so there is little qualitative understanding of the properties of the QGP. It is thus essential to first understand the bulk and transport properties of such matter in a statistical manner. There now exists two domains of QGP, namely the strongly coupled, or weakly coupled QGP (sQGP, wQGP, respectively) whose properties are quite distinct. Whereas the viscosity of sQGP is like that of an ideal gas, its entropy density jumps discontinuously to allow for the display of perfect fluidity, for the wQGP, less ideal fluid behavior is observed as the entropy density drops faster than the viscosity of wQGP [**8**].

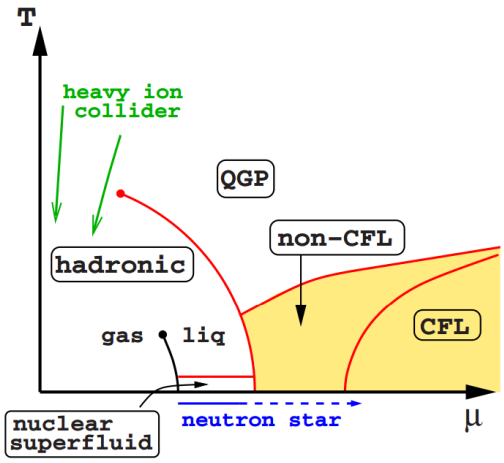

Figure 2.1: Temperature vs. baryon density for QCD-matter. Research suggest we are dealing with a crossover deconfinement in heavy ion collisions [**11**], while there are also possibilites for both first and second order phase transitions. For relatively low temperatures and high baryon density, there exists yet another form of matter, the color flavor locked (CFL) phase [**12**].

Studies of QCD at large baryon densities and low temperature predict the existence of color superconductivity in a phase known as Color Flavor Locked (CFL), a degenerate Fermi gas of quarks with a condensate of Cooper pairs near the Fermi surface inducing a color Meissner effect. In this phase, the quark-matter is an electromagnetically insulating superfluid expected to break chiral symmetry. [**12**]. We are currently exploring the high-temperature-low-density region in heavy ion collisions, where a crossover deconfinement takes place at a quasi-critical temperature of 150 MeV. In FIG.1 is the QCD phase diagram as established in perturbative QCD, which applies to both the high-temperature-low-density and low-temperature-high-density regions. As the hot and dense matter cools and expands, it traverses the hadronic gas-QGP phase transition to equilibrate to normal nuclear density.

2.2 Hydrodynamics and Heavy Ion Collisions

One of the great successes in the field of relativistic heavy ion collisions over the last decade is the prediction of the strong elliptic flow at the Relativistic Heavy Ion Collider (RHIC) and Large Hadron Collider (LHC) using ideal, inviscid hydrodynamics. RHIC announced a strongly coupled quark-gluon plasma formed in Au+Au at $\sqrt{s_{NN}} = 200$ GeV per nucleon collisions, characterized by significant charmonium and meson transverse momentum suppression [**13**]. It is certain we are dealing with the formation of a quark-gluon plasma (QGP) in equilibrium.

The rigorous analysis made using an analytic blastwave model with a strongly coupled quark-gluon plasma core with a dissipative hadronic corona suggests the QGP owes its superfluidity to a sudden increase in entropy density as deconfinement sets in – and not the expected spontaneous lowering of the QGP viscosity. The ratio η/s determines a fluids ability to convert internal energy to collective flow, so a rapid change in s with η almost constant will drive the ratio toward its minimum conjectured limit(s). Ref. [**8**] provides crucial insight into the interpretation of the data collected at RHIC in terms of a hybrid model.

Although the QGP has been established, and event-plane correlations coupled with anisotropies in the transverse plane have established its ratio of η/s to be of order unity larger than the Anti de-Sitter/Conformal Field Thory duality (AdS/CFT) or Heisenberg uncertainty lower limits, still there are as many questions as there were before [**14**]. Hydrodynamical calculations suggest a large range of values, many of whch are able to reproduce central observables, like the strong elliptic flow. Some research suggests all flow harmonics are initially large (direct, elliptic, triangular, etc.), but that only the leading two or perhaps three yield observable signals at kinetic freeze-out [**15**]. The study of higher order harmonics, or perhaps other modes of decomposing the multiplicity seems prudent [**15**, **16**].

The previously assumed inviscid QGP has a finite value of η/s, thus demanding we treat the situation more carefully. Further experiments are needed to better understand viscous effects, both in the QGP phase and the hadronic phase. With the emerging paradigm of viscous hydrodynamics, there is also great interest in the modelling of initial states[**16**, **17**], and the customary decomposition into azimuthal modes may also need revision, to allow for more propagating modes. Probing the properties of the established plasma is a key priority in heavy ion physics. The color-deconfined plasma may also open for extensive studies into QCD interactions [**18**, **19**, **20**, **21**, **22**]. The Chiral Magnetic Effect (CME) has come under extensive theoretical interest in the context of heavy ion collisions. Its counterpart, the chiral vortaic effect (CVE) may also make an apparence in relativistic heavy ion collisions. These effects arise from the axial anomaly, the local violation of discrete symmetries (charge/parity) in QCD. This may lead to baryon charge or strangeness separation and it has been explored using an effective Lagrangian which, when it couples to the electromagnetic field, also couples to an arbitrary field of any conserved charge.

Using event-plane correlators, the effects on the Λ polarization arising from the coupling of vorticity to the strange quark axial current via the strangeness chemical potential was explored. The event-plane correlations were suggested to further establish the value of η/s through the examination of non-linear hydrodynamical responses in Fourier azimuthal modes for higher-order flow harmonics for differing event-plane phases [**23**]. A Fourier-Bessel expansion proposed to examine flow patters in more detail may lead to better understanding of both initial states and final-state anisotropies [**16**, **24**]. Both Glauber and color-glass condensate initial states are able to reproduce multiplicity, flow patterns, and yield ratios within ranges of the conjectured η/s. In Ref. [**17**], a value

of $\eta/s = 0.08 \approx 1/4\pi$ successully reproduced multiplicity, directed, and elliptic flow of charged hadrons. However the large uncertainty stemming from the theoretical and experimental uncertainties surrounding its proper establishment left open the possibility to reproduce the same observables with other values of η/s. The uncertainty given is of the order of the estimate itself.

A key component to the elliptic flow is the participant plane eccentricity, and thus the distribution of nucleons within the nuclei. This has been studied in the wounded nucleon approach using various density distributions for the nucleons in a hybrid model. The strong coupling between the elliptic flow and participant eccentricity lead to the proposal to measure the eccentricity-weighted integrated elliptic flowand its dependence on the impact parameter. Its studies have led to the discovery that v_2/ϵ is a function of multiplicity density [**25**] independent of the details of the participant eccentricity, which could give detailed information about the specific shear viscosity η/s

The magnitude and effects of shear flow in the reaction plane must be examined in more detail. In particular in peripheral heavy ion collisions, the initial angular momentum may lead to vorticious flow due to the shear flow in the reaction plane. Hydrodynamical calculations with non-vanishing viscosity have shown that the longitudinal shear flow can lead to turbulent phenomena, particularly the onset of a Kelvin-Helmholtz Instability (KHI) [**26**, **27**]. The initial results using a definition of circulation fit for relativistic fluiddynamics explored in the non-ideal fluid dynamical paradigm [**10**] show a strong dependence on both the impact parameter and whether conditions are favorable to KHI's. It is pointed out that the strength of the signal is contingent on the centrality, as more peripheral collisions lead to greater vorticity. The observation of vorticity in the late stages of the fluid dynamical evolution could give detailed information about the transport properties of the QGP, but would require precision measurements as the vorticity is sensitive to the explosive expansion of the fluid.

Eventually, when rotational equilibrium has been achieved, the energy of rotation transfers to the explosive expansion of the system, and rotation slows, as was explored in a series of papers recently [**27**, **28**]. As we have seen, vorticious flow plays a role in the studies of polarization in that it may couple to the strange quark axial-current, polarizing the strange quarks. It is pointed out that the CVE is negligible compared to the vorticity arising from conditions favorable to KHI's at large impact parameter; it will be interesting to see how the results of the calculation change now that it is know that the vorticity may have been underestimated for the purposes of peripheral heavy ion collisions.

It is also interesting to note that studies of turbulent phenomena take place in lattice QCD as well, to better understand the thermalization process [**20**, **21**]. Here it is found that in the limit of weak coupling at very high energy employing lattice simulations of the classical Yang-Mills equations, the dynamics of the longitudinally expanding plasma is independent of the details of the initial conditions.

2.3 Polarization in Heavy Ion Collisions

The strong transverse polarization of hyperons that has been observed in inclusive channels in unpolarized beams since the 1970's is still under investigation [**29**]. Early experiments notes that the Λ, ξ, and $\overline{\xi}$ are polarized in the negative y- direction, Σ and $\overline{\Sigma}$ in the positive, while $\overline{\Lambda}$ and Ω display no significant polarization. In particular, studies of Λ^0 in hadron collisions are particularly extensive due to its self-analyzing decay mode into $p + \pi^-$.

Changes in hyperon polarization were one of the earliest suggestions for probing the hot and dense nuclear matter in heavy ion collisions; if the strong transverse polarization observed in nucleon-nucleon and nucleon-hadron collisions makes an appearance in heavy ion collisions, it may indicate the critical QGP formation density is reached. It may also give vital clues into transport properties of QGP. Since then, attempts have been made to establish a mechanism by which polarization may arise. Spin-orbital-momentum coupling in QCD predicts global transverse polarization originating from the quark content of secondary produced hyperons to vanish at high transverse momenta, yet remain strong for p_T of a few GeV/c. Furthermore, secondary produced hyperons may rescatter to aquire polarization during later hadronic stages. If the QGP interacts strongly, it will have many observable effects, like polarized thermal photons, or an effect similar to single-spin left-right asymmetries in $p+p$ collisions . Assuming the strange and non-strange quarks have similar polarizations, the weakly decaying, self-analyzing hyperons are particularly interesting [**30**, **31**, **32**, **33**, **34**, **35**, **36**].

A global transverse polarization of seconday produced hyperons was estimated to be 30% in an exclusive recombination scenario; a more moderate estimate of -0.03-0.15% was predicted using a hard thermal loop with a Debye screening potential, depending on temperature. However, according to data

Λ and $\overline{\Lambda}$ in $\sqrt{s_{NN}} = 62.4$ and 200 GeV/A Au+Au collisions analyzed by the STAR collaboration, there is no global polarization. Having averaged over significant centralities (0-80% and 20-70%, respectively) and over the azimuthal of the momentum direction of the Λ, no more than 2% was observed [**37**].

Thus the search for a possible signal continues. Following the ideas of [**33**, **34**], Ref. [**38**] investigates multiple quark-quark scattering in the global polarization scenario. Leaving open the possibility for an quark initial polarization, the time dependence of the quark polarization is examined in a laminar flow governed by viscous hydrodynamics. The quark polarization is found to always point in the negative y direction within the small angle approximation. It is inversely related to η/s with a strong dependence on the initial shear of local longitudinal flow, and on the transverse expansion as demonstrated by contrasting stationary and boost-invariant boundary conditions. In viscous fluid flow, initial longitudinal shear flow may lead to parton pairs with non-vanishing impact parameter having relative local orbital angular momentum along the direction opposite to the reaction plane. This can lead to global quark polarization within both Landau fireball and Bjorken scaling model of initial parton production.

Quarks polarized through quark-quark scattering via the exchange of a thermal gluon was also calculated beyond the small angle approximation in QGP, and is shown to display a non-monotonic dependency on the relative local orbital angular momentum. The dependecy is dictated by interplay between electric and magnetic interactions [**39**]. It it hard to establish how the value for quarks, $|P_q| < 0.04$ relate to the hadrons with respect to agreement with the measurements performed at RHIC.

Ref. [**40**] investigates the transverse hyperon polarization by examining its coupling to the thermal vorticity, defined as

$$\varpi^{\mu\nu} = \frac{1}{2}(\partial^\nu \beta^\mu - \partial^\mu \beta^\nu). \tag{2.1}$$

Here $\beta^\mu(x) = u^\mu(x)/T(x)$ is the inverse temperature field, and u^μ is the flow four-velocity. T is the temperature. Using a Cooper-Frye freeze-out formalism adapted to fermions, provided spin degrees of freedom locally equilibrate, transverse polarization of secondary produced hyperons arises from any change in the inverse temperature field. In particular, a careful selection of Λ transverse momentum lying in the reaction plane will lead to significant transverse polarization of secondary produced hyperons.

Now more than ever, the transverse polarization of secondary produced hy-

perons in hadron collisions is strong [**41**], but a clear signal remains to be seen in heavy ion collisions. Though it is itself an indication of the reabsorption of secondary produced particles into the sQGP phase, thus confirming it has formed, some signal would be very interesting indeed. In Ref. [**42**], the first results using the exact model proposed in a series of papers culminating in a new, exact family of solutions to fireball hydrodynamics with anisotropic Hubble flows and scaling temperature and density profiles was reported. The transverse polarization arising from the curl of the inverse temperature field was around 10%. Though consistent with our results, we show the assumption that the gradient of the inverse temperature field is negligible was mistaken. Here we calculate the polarization term due to the gradient of the inverse temperature as well, and present the very first results for the polarization of secondary produced Λ's in the non-relativistic limit using a cylindrically symmetric fireball in the context of *Case 1*$\mathcal{A}$ from [**43**].

Chapter 3

Some General Ideas

3.1 General Remarks

There are many things to consider: If the polarization arises from the curl and gradient of the inverse temperature field, then collective motion, especially the differential elliptic flow $dv_2(p_T)/dp_T$ attained through azimuthal correlations and differential HBT analyses [**44**] will be important to detect the rotation. A careful understanding of the interplay between internal energy and axial/radial expansion is also important [**28**]. This again leads to the need for a more subtle understanding of event-by-event fluctuations in participant event plane eccentricity, interferomtery, initial states, transport properties, and so on. We must also seek to understand the transparency effect displayed in ultrarelativistic collisions, which may serve to further restrict the QGP equation of state (EOS); this is the constituent relation containing all the pertinent bulk properties as they relate to statistical ensembles within the fluid particles and which, at least in the case of perfect fluid dynamics, closes the system of equations allowing for an attempt to solve; in fact, many hydrodynamical models use the elliptic and directed flow parameters to constrain their equations of state [**45**, **46**]. The equation of state may also be influenced by important work looking into the properties of the EOS of normal nuclear matter [**47**].

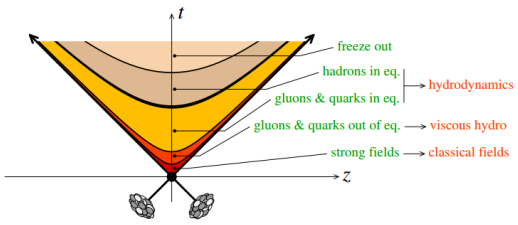

Figure 3.1: The evolution stages of heavy ion collisions [**50**].

The evolution of an event in a heavy ion collider is depicted in FIG.1. We see the soft probes, thermal photons and and lepton pairs, originating in the sQGP phase and leave the reaction zone immediately. These give information of the bulk properties of QGP. The hard probes must penetrate the hot and dense plasma, and thus provide information about its transport properties. Reabsorption accounts for asymmetries in particle p_T spectra, as well as a possible suppression of charm bound states, like the J/Ψ.

In heavy ion collisions, many fields of physics coalesce. We use quantum mechanics to calculate the probabilities related with the properties of particles and their interactions. So there are expectation values associated with measuring those properties. Furthermore, we cannot use one collision to examine our assumptions and predictions, so we average over many events as well. Statistics plays a large role in our collecting data. Everything takes place in the space-time continuum, so invariance plays a large role in attaining the correct data for a given measurement. The properties of particles related to position and momenta are relatively easy to handle; those symmetries and relations taking place in the "more" complex Hilbert spaces are very complicated, indeed, and are formulated using quantum field theory with complex internal symmetries and interactions.

There are also many fields of inquiry related to hydrodynamics in relativistic heavy ion collisions, many of which pertain to polarization. The hydrodynamics need elaborate inital states describing the initial velocities and entropy density. The most used states are Glauber states or color-glass condensates. These are coherent, minimal uncertainty states, and transiently solid, highly length-contracted gluon saturated nuclei, respectively. The QGP appears an almost perfect fluid as it has bee successfully modelled using the relativistic Euler equations. This is evident in the large azimuthal anisotropies. However, viscous corrections to the ideal, inviscid hydrodynamics are becoming increasingly im-

portant. When considering most observables, hybrid fluid dynamics and hadron cascade models have the best ability to reproduce the data from RHIC and LHC. Whereas models assuming chemical equilibrum reproduce hadron abundances and radial flow at the expense of differential elliptic flow, models assuming partial chemical equilibrium reproduce the latter to the detriment of the former two. Although hybrid models still struggle with energy and momentum conservation due to the interface between the sQGP core and the hadronic resonance gas phase, they seem the best approach in the light of the properties displayed.

3.1.1 On Initial States

With higher energies there is a need to specify the intial states in increasing detail, and therefore the need for a better understanding of event-by-event fluctuations in the initial conditions. These form the input in fluid dynamical (+cascade) models, and are for instance Glauber states, or color-glass condensates (CGC). Glauber states are general quantum mechanical states that are eigenvectors of the annihilation operator. As we have seen, these states display classical behavior, and form a good starting point for a hydrodynamical scheme. Although only alluded to in the previous section, the fluid dynamical properties of the initial fluid flow are encoded in these states [**48**, **49**].

The CGC is a transient solid state which is predicted to dominate for length-contracted nuclei in relativistic heavy ion collisions. First proposed in DIS experiments to explain the parton distribution function of nucleons, it has since been successful in describing the incident nuclei. As the gluon density exceeds the QCD momentum saturation scale, the effective coupling is such that it allows pertubative expansion in terms of free quark and gluon fields and light-like color sources. For the duration of the interaction, the timescales are an 2-3 orders of magnitude longer than in the nucleon at rest (RHIC, LHC, respectively), so the color fields are treated classicaly. In this regime, the picture of the three valence quarks gives way to a more complicated picture in which a sea of QCD interactions take place. Owing to the large density of gluons in the nucleus, it may be viewed as a static color condensate, since the fields are not really static. These then form the basis for the classical Yang-Mills color fields which develop in a so-called glasma until conditions suitable for hydrodynamics treatment arises.

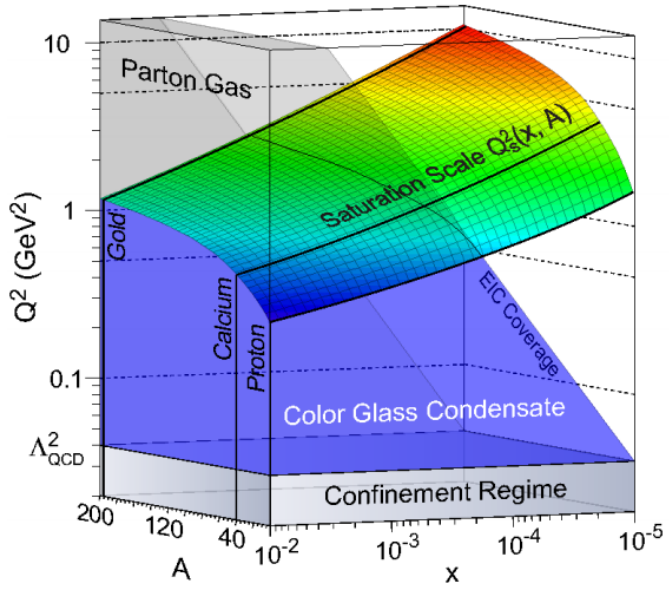

Figure 3.2: The gluon saturation scale Q_s^2 as a function of nucleon number, A, and Feynman x, $x = p_z/\sqrt{s}$. The color-glass condensate allows for perturbative treatment of interactions between color charges [**50**]

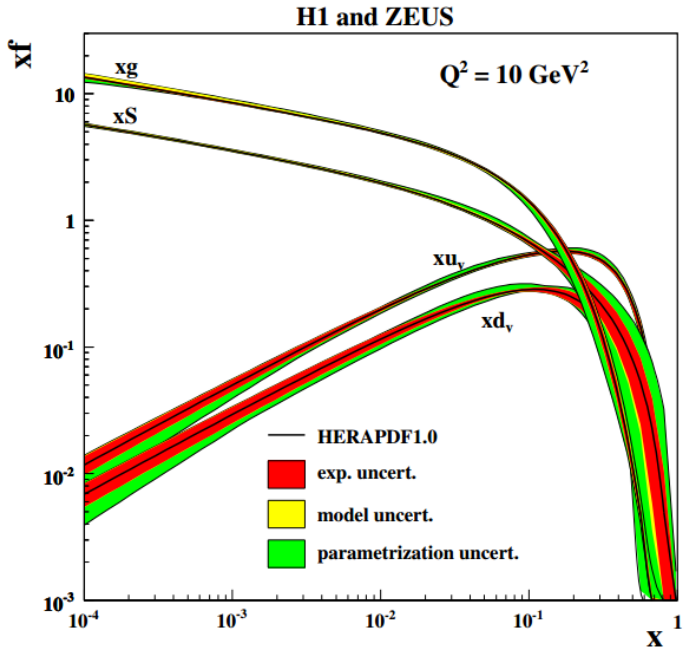

Figure 3.3: The parton distribution of a proton resulting from Deep Inelastic Scattering experiments. As the fraction of nucleon momentum carried by the different parton flavors, $x = p_z/\sqrt{s}$, diminishes, more and more QCD interactions take place, until the dynamics of the nucleon is completely dominated by gluon interactions. The sea quarks are an order of magnitude less likely than gluons, thus the gluons dominate the nucleon dynamics in high-energy collisions [**50**].

The coordinate system mostly used in heavy ion collision physics is one in which the beam direction is along z, and the reaction plane is spanned by $\hat{z}$ and the impact parameter $\boldsymbol{b}$ defined to be the distance separating the nuclei in the reaction plane. The transverse plane is the xy-plane. However, the distribution of nucleons is not homogeneous within the nuclei, thus their configuration defines the event planes depicted in FIG. 5. The initial states of peripheral heavy ion collisions are thus prone to fluctuations. These fluctuations, including fluctuations arising from individual collisions between nuclei may be encoded into the initial state via a Glauber state or Glasma. The initial eccentricity has been shown to lead to significant eccentricity in hadron p_T spectra as predicted by the customary Fourier analysis of azimuthal modes.

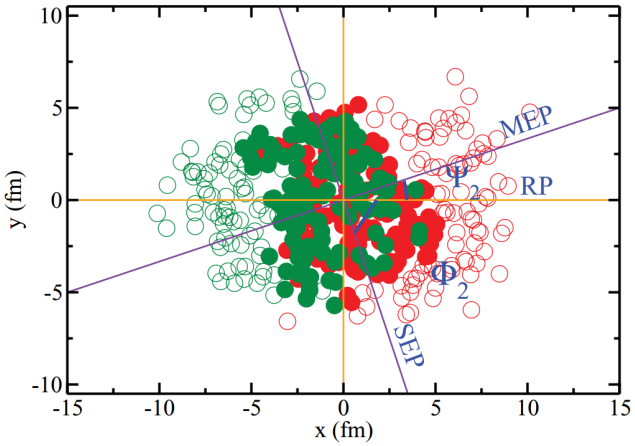

Figure 3.4: Depicted is the event plane in the initial configuration of nucleons within the colliding nuclei. The customary flow harmonics use the momentum event plane angle (here) Ψ_2. The filled circles represent participant nucleons; the empty are spectators [**15**]. The *participant* plane is randomly tilted with respect to the reaction plane.

Most often studied is the set of flow harmonics coefficients $\{\langle v_n \rangle\}$ of the azimuthal Fourier expansion of the Cooper-Frye kinetic freeze-out formula,

$$E\frac{dN}{dp^3} = \frac{1}{2\pi}\frac{dN}{p_T dp_T dy}\left(1 + \sum_{n=1}^{\infty} 2v_n \cos\left[n(\phi - \Psi)\right]\right). \tag{3.1}$$

Here E, p_T, y, and ϕ are energy, transverse momentum, rapidity, and azimuthal emission angle with respect to the positive x-axis, respectively; Ψ is the angle of the reaction plane. The coefficients of the cosine in the series give rise to the names directed v_1 flow, elliptic v_2 flow, triangular v_3 flow, etc.

As a sidenote, there is strong correlation between η/s and flow harmonics, and thus, eccentricity in the initial state. Yet the fact that participant plane is sensitive to fluctuations about the reaction plane, the correlation is not very precise in estimating η/s. It should also be noted that the reaction plane is not observable, so it must be inferred from the the symmetry properties of the flow. For this one may use azimuthal correlations to average over an event and subsequently over all events. This way one may infer the reaction plane for a given centrality.

In Ref. [**16**] a new approach to the study of collective motion is proposed. They propose to use Bessel-Fourier series instead of the simpler Fourier series. This may prove essential for further understanding of the flow properties of QGP, as it allows for expansion in terms of radial modes as well as the familiar azimuthal modes. Within 1% accuracy the enthalpy distribution in an initial state in the wounded nucleon Monte Carlo Glauber is reproduced. In Fig. 4 the number of included modes are the same for both modalities, and the number of modes are chosen to be $6, 10, 15, 20$, and 30. An almost exact replica is found when the initial conditions in a random Pb+Pb collision is reproduced.

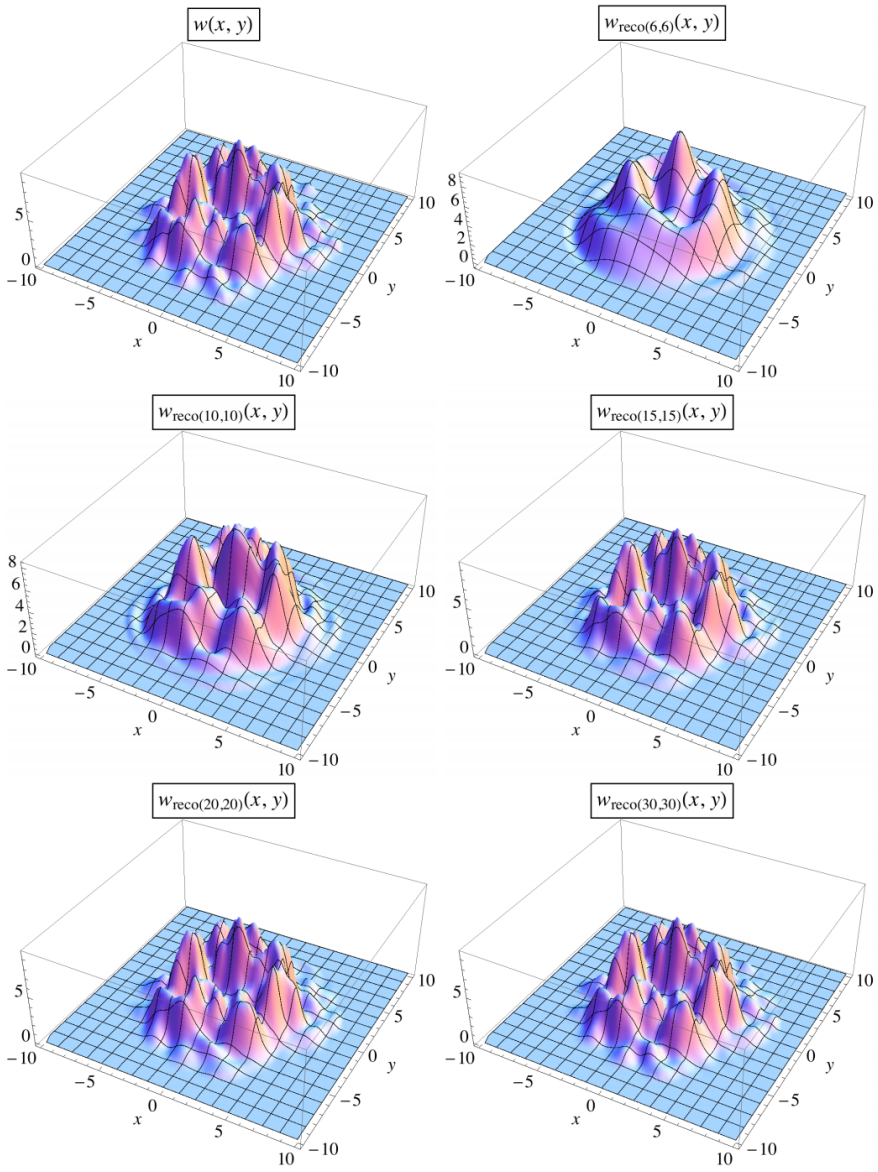

Figure 3.5: The initial transverse enthalphy distribution, $w(x, y)$, as produced by a Monte Carlo Glauber model in which the enthalpy is proportional to the number of wounded nucleons in the upper-left corner. The remaining plots are the reproduced transverse enthalpy distributions for an increased number of terms from the Fourier-Bessel series [**16**].

Chapter 4

Λ Polarization in Heavy Ion Collisions

Λ Polarization in an Exact Rotating and Expanding fluid dynamical model for peripheral heavy ion reactions

Yilong Xie, Robert C. Glastad, László P. Csernai
Institute of Physics and Technology, University of Bergen, Allegaten 55, 5007 Bergen, Norway
(Dated: May 28, 2015 - v6)

We calculate the Λ polarization in an exact analytical, rotating model based on parameters extracted from a high resolution (3+1)D Particle-in-Cell Relativistic hydrodynamics calculation. The polarization is attributed to effects from thermal vorticity and for the first time the effects of the radial and axial acceleration are also studied separately.

PACS numbers: 25.75.-q, 24.70.+s, 47.32.Ef

I. INTRODUCTION

In high energy peripheral heavy ion collisions there is a substantial amount of initial angular momentum present directly after the Lorentz contracted nuclei penetrate each other, and proceed to fill the reaction zone with a hot and dense soup of elementary particles forming a relatively new state of matter – the quark-gluon plasma (QGP) – consisting of unbound quarks and gluons in a confined system. Subsequently the plasma expands and cools according to statistical laws in continuum mechanics and thermodynamics with implied local thermodynamical equilibria, followed by a final kinetic transport development determined by cross-sections between neighboring fluid particles.

Due to a finite impact parameter, the initial stage (IS) may have a non-vanishing angular momentum [1, 2]. In the initial stages, effective models as a color glass condensate (CGC) [3] or Glauber states [4] are used. In general, the IS uses experimental data, to construct a possible IS using participant nucleons, eccentricity, and impact parameter. Early studies neglected effects arising from the non-vanishing angular momentum, but interest increased recently [5, 6].

After many decades of refinement [7, 8], solutions of fireball hydrodynamics, the hydrodynamics best suited to describe the system that arises in peripheral heavy ion collisions at relativistic energies. Thus, rotation and its consequences were studied as well [9, 10].

We look at polarization in effects arising from thermal vorticity in an exact rotating model, modelling an appropriate time-period of the collision. Special attention has been given to collective motion to extract it from observables, which could confirm that such descriptions are indeed plausible.

We calibrate an exact rotating model based on a (3+1)D fluid dynamical model, the relativistic particle-in-cell method (PICR), to fine-tune the initial parameters of the rotating and expanding fireball. Other methods include the three-fluid (3FD) approximation model, in which modelled are the distributions of two constituent fluids, one for each of the colliding nuclei, and one for the "fireball" fluid developing in a given transition time [11, 12]. These models assume QGP formation. The dynamical effects of QGP in the Equation of State (EoS) is studied for a long time [13].

In Ref. [14] the differential Hanbury Brown and Twiss (HBT)-method was used to detect rotation in heavy ion collisions. The HBT method was proposed to measure the size of a system – initially stars for cosmological purposes [15], yet the method has "morphed" into a tool to detect and analyze rotation in sources varying from giant stars to tiny particles using emission functions and correlation functions.

Furthermore, studies of the relationship between shear viscosity and entropy have shown that the development of strong collective effects like transverse and azimuthally asymmetric flow, or "elliptic" flow, which imply an almost perfect fluid dynamic for the early stages in which these effects are thought to be produced [16].

Without at least some viscosity, however, there would be no rotation, so we now assume QGP to be a near-perfect fluid. Although perturbative quantum chromodynamics (pQCD) does not show significant improvement in trying to account for these effects, an effective Van der Waals excluded volume hadron-resonance gas may be capable of producing the desired result in a hydrodynamical description given hard-spheres of sufficient radii ($r \geq 0.2$), to account for the ratio of shear viscosity to entropy density, η/s, for the time being thought to be bounded below by $\hbar/4\pi k_B$ [17].

Thermal vorticity arises from the inverse temperature field present in heavy ion collisions, and it arises mainly due to a non-vanishing angular momentum in the initial stages, but in the transverse plane fluctuations can achieve significance for the measurement [18] one may wish to perform. It may also be further enhanced by the Kelvin Helmholtz Instanolity (KHI) evolving in the period prior to equilibration of rotation.

In our formalism, the dynamics of the system prior to equilibration is computed using a (3+1)D fluid dynamical model based on the particle-in-cell method. This fluid dynamical computation shows enhanced collective rotation due to an evolving KHI. In Ref. [19] an effective model for this phenomena is explored using a few material properties: the surface tension between the colliding nuclei, the viscosity, and the thickness of the flow layer. This enables a classical potential flow approximation, in

which one may study the dynamics of an onsetting KHI.

A more recent calculation of the onset and effects of the KHI is performed in Ref. [20], in which the calibration of the exact model takes place. Here it is pointed out that this feature – the enhancement of rotation – is a dominant aspect of the (3+1)D fluid dynamical model, but it is also seen in UrQMD [21].

There has also been progress in other fields pertaining to heavy ion collision, and in nuclear physics, new modes of resonance have been suggested to account for asymmetric densities in the nucleus itself. Itself paving way for better understanding the so-called "magic numbers", the study may also have profound implications for the equation of state (EoS) governing the matter in collisions.

In Ref. [22], the authors take a closer look at the low-energy E1 model, accounting for several shifts in energy due to both mean fields and residual interactions, as well as electromagnetic interactions. These correspond to the pygmy dipole resonance, the toroidal resonance, and to anisotropic compressional resonance modes [23].

In Ref. [24], a discrepancy between the hydrodynamic definition of vorticity, $\overline{\omega} = \nabla \times \boldsymbol{v}$, and the "Raventhall-Wambach vorticity" is explored to propose indicators for nuclear vorticity. In the article, the toroidal strength approximation is used instead of the hydrodynamical definition, as it decouples from the continuity equation in the Raventhall-Wambach definition of vorticity, exhibiting a natural vorticious flow.

At high energy collisions, initially prior to both the (3+1)D fluid dynamical model and the subsequent exact analytical, rotation model, the collision is forming a color-glass condensate (GCG), after that we have expanding fire streaks, which can be described by Yang-Mills fields acting between color charges. Our exact model starts a short time after a (3+1)D fluid dynamic stage, which uses as initial condition the result of the fire streak Yang-Mills field action and the subsequent initial fluid dynamical development of nearly uniform rotation.

Proposed in Ref. [25] there are two families of exact analytical, rotating solutions, of which one is the subject of this, and other papers, in attempts to familiarize ourselves with new phenomena arising due to the solutions – and how they fit together with known and preferably unknown observables.

In Ref. [25] an ansatz for the velocity field $\boldsymbol{v} = \boldsymbol{v}_H + \boldsymbol{v}_R$ is set forth, with $\boldsymbol{v}_H$ being the irrotational velocity field, while $\boldsymbol{v}_R = (\boldsymbol{\nabla} \times \boldsymbol{v}) \times \boldsymbol{r} \equiv \boldsymbol{\omega}(t) \times \boldsymbol{r}$ is the rotational velocity field. Hubble flows are now an integral part of the velocity field, encoded in the irrotational field. With these assumptions, one assumes an equation of state and pursues solutions as best one can. Ref. [25] then proceeds to define the two different families based on the physical properties of the collision (whether there is a conserved number density or not) and the proceeds to outline different cases for each family of solutions. A set of scaling variables,

$$(s_R, s_Y) = \left(\frac{x^2 + z^2}{R^2}, \frac{y^2}{Y^2} \right), \tag{1}$$

is also proposed with $s = s_R + s_Y$ being the scaling variable as it appears in the thermodynamical relations. Here we have interchanged the y- and z-axes to resonate with choice of axes in heavy ion collision literature, in which the reaction plane, in which the system rotates, is spanned by $\boldsymbol{e}_x$ and $\boldsymbol{e}_z$, leaving the axis of rotation to be defined by $\boldsymbol{e}_y$.

Ref. [20] provides an extensive look at the simplest case from the aforementioned paper, and proceeds to calibrate the exact model to the (3+1)D fluid dynamical model which precedes it in time, extracting parameters from experiments at $\sqrt{S_{NN}} = 2.76A \cdot TeV$ with impact parameter $b = 0.7 b_{Max}$ (See Fig. 1 and 2). In the (3+1)D models, rotation increases due to Kelvin-Helmholtz instabilities, whereas in the exact model – and the later stages in the experiments themselves – rotation slows due to a transfer of energy to the explosively increasing size of the system after a period of time. The exact model, therefore, is suited to describe the period after the equilibration of rotation in the (3+1)D model, but prior to the freeze-out, in which rotation slows down.

From [25] case 1A, the solution for a flow of conserved number density together with a constant, temperature-independent compressibility in the velocity field is proposed, hence the solutions take the forms, in cylindrical coordinates (r, y, ϕ), where $r = \sqrt{x^2 + z^2}$ with equation of motion $\dot{\boldsymbol{r}}(t) = \boldsymbol{v}(\boldsymbol{r}, t)$. The exact model assumes a linear velocity both in the radial, r, and in the axial, y, directions. This result in a flow development where a fluid element starting from a point (r_0, y_0, ϕ_0) at a later time, t reaches the point

$$\begin{aligned} r(t) &= r_0 \frac{R(t)}{R(t_0)}, \\ y(t) &= y_0 \frac{Y(t)}{Y(t_0)}, \\ \phi(t) &= \phi_0 + \int dt\, \omega(t), \end{aligned} \tag{2}$$

showing explicitly how the solutions evolve in time, rotating and expanding together with the fluid; they also follow the time-evolution of the scaling variables in the radial and axial directions. This is a Cylindrically symmetric setup with $X(t) = Z(t)$, $\sqrt{X^2(t) + Z^2(t)} = R(t)$ and, in general, $Y(t) \neq R(t)$.

We have chosen the xz-plane as our reaction plane, with y the axis of rotation; our initial angular momentum, then, points in the negative y-direction, with an absolute value of approximately $1.45 \cdot 10^4 \hbar$. In an attempt to determine new observables, we propose a search for Λ polarization. Our hope is that this polarization, at least in part, will be able to account for the polarization as observed in peripheral regions in the first 10-15fm/c following an impact in a heavy ion collider.

In Ref. [26] the energy weighted thermal vorticity in the exact model with the parameters found in Ref. [20] was calculated. First explored was the total energy of the system and the energy of each relevant component and how they changed in time, showing an expected transfer of energy from rotation to expansion, hence the rotation slows as the system expands up until the freeze-out.

According to Ref. [27], in which a quantum-field-theoretical approach to the Λ polarization in an inverse temperature field $\beta^\mu(x) = u^\mu(x)/T(x)$ is laid out, the expectation value for Λ polarization, $\Pi_\mu(x,p)$, goes as

$$\langle \Pi_\mu(x,p)\rangle = \frac{1}{8}\epsilon_{\mu\rho\sigma\tau}(1-n_F)\partial^\rho\beta^\sigma(x)\frac{p^\tau}{m}, \tag{3}$$

where $\epsilon_{\mu\rho\sigma\tau}$ is the completely antisymmetric Levi-Civita symbol, n_F the Fermi-Jüttner distribution for spin-1/2 particles ($(1-n_F)$ is the Pauli blocking factor), and p is the Λ four-momentum. This we integrate over some volume, ultimately over all of space, weighted by the number density, normalized by number of particles in that volume, leaving a momentum-dependent polarization four-vector in the participant frame of reference

$$\Pi_\mu(p) = \hbar\epsilon_{\mu\sigma\rho\tau}\frac{p^\tau}{8m}\frac{\int d\Sigma_\lambda p^\lambda n_F(x,p)(1-n_F(x,p))\partial^\rho\beta^\sigma}{\int d\Sigma_\lambda p^\lambda n_F(x,p)}\,. \tag{4}$$

Note that, as opposed to electromagnetic phenomena, in which particle and anti-particle will have anti-aligned polarization vectors, here it is shown that Λ and $\bar{\Lambda}$ polarizations are aligned in vorticious flow thermal fields.

While the average values of polarization may be as low as 1-2%, consistent with RHIC bounds, in some regions of momentum space we see a larger polarization, about 5% for momenta in the transverse plane up to 3 GeV/c. Kelvin-Helmholtz instabilities may further enhance rotation, hence thermal vorticity, defined as

$$\varpi_{\mu\nu}(x) = \frac{1}{2}(\partial_\nu\beta_\mu - \partial_\mu\beta_\nu) \tag{5}$$

and thereby increase signal strength by 10-20%. At LHC energies, there may be 5% Λ polarization due to the corona effect, single nucleon-nucleon collisions occurring outside of the reaction zone of the collision itself. So attempts should be made to further the understanding of this background, and remove it from measurements in order to further isolate the Λ polarization as it arises from the collision itself.

The Λ polarization is determined by measuring the angular distribution of the decay protons in the Λ's rest frame. In this frame the Λ polarization is $\mathbf{\Pi}_0(\boldsymbol{p})$, which can be obtained by a Lorentz boosting the polarization $\mathbf{\Pi}(\boldsymbol{p})$ from the participant frame to the Λ's rest frame, Ref. [28]:

$$\mathbf{\Pi}_0(\boldsymbol{p}) = \mathbf{\Pi}(p) - \frac{\boldsymbol{p}}{p^0(p^0+m)}\mathbf{\Pi}(p)\cdot\boldsymbol{p}\,, \tag{6}$$

where $(p^0, \boldsymbol{p})$ is the Λ four-momentum and m its mass.

Based on this equation we see that in order to maximize polarization, we need to choose momenta for the Λ such that they lie in the reaction plane, or transverse to it, hence we fix $\boldsymbol{p}$ in the positive z-direction (beam directed momentum).

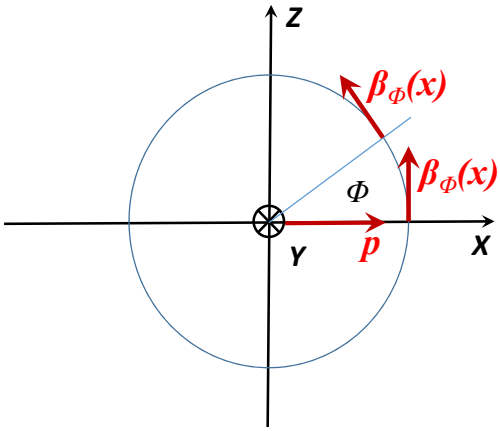

FIG. 1. (color online) The direction of axes, as well as the momentum, $\boldsymbol{p}$, and flow, $\boldsymbol{\beta}$, vectors. The azimuth angle is measured from the direction of the $\boldsymbol{p}$-vector, i.e. from the x-axis.

II. SOLUTION FOR THE Λ POLARIZATION

As the Λ is transversely polarized, $\Pi^\mu p_\mu = 0$, one can confine himself to the spatial part of Π^μ. The simplified spatial part of polarization vector is:

$$\mathbf{\Pi}(p) = \frac{\hbar\epsilon}{8m}\frac{\int dV n_F(x,p)\,(\nabla\times\boldsymbol{\beta})}{\int dV n_F(x,p)} + \frac{\hbar\boldsymbol{p}}{8m}\times\frac{\int dV n_F(x,p)\,(\partial_t\boldsymbol{\beta}+\nabla\beta^0)}{\int dV n_F(x,p)}\,. \tag{7}$$

where n_F is the phase space distribution of Λs, $n_F(x,p)$. In a previous calculation [28], the p depencence of n_F, was considered negligible in the integral and the time derivative and gradient terms were also assumed to be smaller. The present calculation shows that in general these terms are not negligible, and it depends on the particular conditions, which terms are dominant.

A. The denominator

We first perform the integral in the denominator:

$$A(p) \equiv \int dV\, n_F = \int_0^R r\,dr \int_{-Y}^{+Y} dy \int_0^{2\pi} d\phi\; n_F(x,p)\,. \tag{8}$$

According to Eq. (3) in Ref. [26] in terms of the scaling variable, s, we have:

$$n = n_0 \frac{V_0}{V} \nu(s) \ , \tag{9}$$

$$\nu(s) = \frac{1}{\tau(s)} \exp\left(-\frac{1}{2}\int_0^s \frac{du}{\tau(u)}\right) = 1 \cdot \exp\left(-\frac{1}{2}\int_0^s du\right) \ , \tag{10}$$

where the simplifying choice of $\tau(s) = 1$ is used in the last step. Therefore:

$$n(s) = n_0 \frac{V_0}{V} e^{-\frac{1}{2}s} \ . \tag{11}$$

The EoS is assumed to be: $\epsilon(s) = \kappa T(t) n(s)$ and the energy density $\epsilon(s)$ is calculated as in Eq. (29) in Ref. [26], therefore:

$$\begin{aligned} n(s) &= \frac{\epsilon}{\kappa T(t)} \\ &= n_0 \frac{V_0}{V} \frac{T_0}{T} \left(\frac{V_0}{V}\right)^{\frac{1}{\kappa}} e^{-\frac{s}{2}} \\ &= n_0 \frac{T_0}{T} \left(\frac{V_0}{V}\right)^{1+1/\kappa} e^{-\frac{s_y}{2}} e^{-\frac{s_\rho}{2}} \\ &= \frac{C_N}{\kappa T} e^{-\frac{s_y}{2}} e^{-\frac{s_\rho}{2}} \ , \end{aligned} \tag{12}$$

where $C_N = \kappa n_0 T_0 (\frac{V_0}{V})^{1+1/\kappa}$.

From Ref. [28], the Fermi-Jüttner distribution is:

$$n_F(x,p) = \frac{1}{e^{p^\mu \beta_\mu - \xi} + 1} \approx \frac{1}{e^{p^\mu \beta_\mu - \xi}} = \frac{e^{\mu/T}}{e^{p^\mu \beta_\mu}} \ , \tag{13}$$

where the $\xi = \mu/T$, and μ is chemical potential. The thermal flow velocity, $\beta^\nu = \beta^\mu(x) \equiv u^\mu(x)/T$ is different at different space-time points x.

As is known, the invariant scalar density for Jünttner distribution is:

$$n = \frac{4\pi m^2 K_2(m/T)}{(2\pi\hbar)^3} e^{\mu/T} = \frac{e^{\mu/T}}{C_0} \tag{14}$$

where the $C_0^{-1} = 4\pi m^2 T K_2(m/T)/(2\pi\hbar)^3$. With C_0 and $n(s) = n$, the Fermi-Jüttner distribution can be written as:

$$n_F(x,p) = \frac{e^{\mu/T}}{e^{p^\mu \beta_\mu}} = \frac{C_0 n(s)}{e^{p^\mu \beta_\mu}} \ . \tag{15}$$

Now we introduce cylindrical coordinates for the location in the configuration place $x = (r, y, \phi)$, and using the scaling expansion model [20, 25] we introduce the scaling variables $s\,, s_r\,, s_y$. Now, substituting Eqs. (12,15) into the denominator of $\Pi(p)$, i.e. Eq. (8), and noticing that $s = s_r + s_y = \frac{r^2}{R^2} + \frac{y^2}{Y^2}$, one obtains:

$$\begin{aligned} A(p) &\equiv \int dV\, n_F(p,s) \\ &= \frac{C_N C_0}{\kappa T} \int r\, dr \int dy \int d\phi\ n(s)\ e^{-p^\mu \beta_\mu} \\ &= \frac{C_N C_0}{\kappa T} \int_{-aY}^{aY} dy \exp\left(-\frac{y^2}{2Y^2}\right) \int_0^{bR} r dr \exp\left(-\frac{r^2}{2R^2}\right) \\ &\quad \times \int_0^{2\pi} d\phi\, e^{-p^\mu \beta_\mu} \ . \end{aligned} \tag{16}$$

In the above equation, we first integrate with respect to ϕ.

Generally, the position of the integration point in cylindrical coordinates is: $\boldsymbol{x} = (r, y, \phi) = r\boldsymbol{e}_r + y\boldsymbol{e}_y + \boldsymbol{e}_\phi$. The spatial part of momentum vector, $p^\mu = (p^0, \boldsymbol{p})$, in cylindrical coordinates is: $\boldsymbol{p(x)} = (p_r, p_y, p_\phi) = p_r\boldsymbol{e}_r + p_y\boldsymbol{e}_y + p_\phi\boldsymbol{e}_\phi$, and similarly: $\boldsymbol{\beta}(x) = (\beta_r, \beta_y, \beta_\phi) = \beta_r\boldsymbol{e}_r + \beta_y\boldsymbol{e}_y + \beta_\phi\boldsymbol{e}_\phi$. Then the scalar product is $p^\mu\beta_\mu = (p^0, \boldsymbol{p})(\beta_0, \boldsymbol{\beta}) = p^0\beta_0 - \boldsymbol{p}\,\boldsymbol{\beta} = p^0\beta_0 - p_r\beta_r - p_y\beta_y - p_\phi\beta_\phi$.

In our integral the p^μ is given or 'fixed' as the argument of $\boldsymbol{\Pi}(p)$, while the $\boldsymbol{\beta} = \boldsymbol{\beta}(x)$ is changing. The integration with respect to ϕ starts from the direction of the $\boldsymbol{p}$-vector. According to the Eq. (5) in reference [26]: $\boldsymbol{v} = v_r\boldsymbol{e}_r + v_\phi\boldsymbol{e}_\phi + v_y\boldsymbol{e}_y = \frac{\dot{R}}{R} r\boldsymbol{e}_r + \omega r\boldsymbol{e}_\phi + \frac{\dot{Y}}{Y} y\boldsymbol{e}_y$, and $\boldsymbol{\beta} = u^i/T = \gamma\boldsymbol{v}/T$, thus in the integral for ϕ we exploit that in the exact model we discuss, the radial, r, and axial, y, components of the thermal velocity, $\boldsymbol{\beta}$, do not depend on ϕ, while the tangential component does not depend on y, i.e. $\beta_\phi = \gamma r\,\omega/T$, but its direction is changing with respect to the direction of $\boldsymbol{p}$. As the integral is over the whole 2π angle we can start it at any point of ϕ, so we start it from the extremely given $\boldsymbol{p}$-direction. Consequently, with this choice of the x-axis, $\boldsymbol{p} = (p_r, p_y, 0)$, and $p_z = p_\phi = 0$. In this azimuthally symmetric, exact model it is sufficient to calculate $\Pi(\boldsymbol{p})$ for one direction of $\boldsymbol{p}$ in the $[x, z]$-plane.

For the volume integration we still have to integrate over the azimuthal direction ϕ. The $\boldsymbol{p}\cdot\boldsymbol{\beta}$ product will be the same for every azimuthal angle as at the x-axis.

The direction of the thermal velocity is tangential to the direction ϕ, i.e. it points to the $\boldsymbol{e}_{\phi+\pi/2}$-direction.

Thus the scalar product is:

$$\boldsymbol{p}\cdot\boldsymbol{\beta}(r,\, y, \phi) = |p_x|\beta_r \cos(\phi) + p_y\beta_y + |p_x|\beta_\phi \cos\left(\phi + \frac{\pi}{2}\right) \ ,$$

where ϕ is the azimuth angle of the position around the y, rotation axis, counted starting from the x-axis. Thus we have chosen the coordinate axes in a way that the $\boldsymbol{p}$ is orthogonal to the z axis, $p_z = 0$. So, the integral starts from $\phi = 0$, when $\boldsymbol{p}$ and $\boldsymbol{\beta}_\phi$ are orthogonal. See Fig. 1.

So, inserting the last expression for $p^\mu\beta_\mu$ into the last term of the integral Eq. (16), the integral with respect

to ϕ will take the form:

$$\int_0^{2\pi} d\phi\, e^{-p^\mu \beta_\mu} = e^{-\gamma p^0/T}\, e^{p_y \beta_y} \times \int_0^{2\pi} d\phi\, e^{|p_x|\beta_r \cos(\phi) - |p_x|\beta_\phi \sin(\phi)} = \int_{-\pi}^{\pi} d\phi\, e^{a\cos(\phi) - b\sin(\phi)} = 2\pi I_0\left(\sqrt{a^2+b^2}\right), \quad (17)$$

where $a = |p_x|\beta_r = |p_x|\gamma \dot{R} r/TR$ and $b = |p_x|\beta_\phi = |p_x|\gamma r\,\omega/T$, and we used integral no. 3.338(4) [29]. If we define

$$c_3 = \sqrt{\left(\frac{p_x \gamma \dot{R}}{TR}\right)^2 + \left(\frac{p_x \gamma\, \omega}{T}\right)^2} = \frac{|p_x|\gamma}{T}\sqrt{(\dot{R}/R)^2 + \omega^2}\,,$$

then $\sqrt{a^2+b^2} = c_3 r$, and:

$$\int_0^{2\pi} d\phi\, e^{-p^\mu \beta_\mu} = e^{-\gamma p^0/T}\, e^{p_y \beta_y} \times 2\pi I_0\left(c_3 r\right). \quad (18)$$

Now, substitute this back into Eq. (16):

$$\begin{aligned} A(p) &= \int dV\; n_F(p,s) \\ &= \frac{C_N C_0}{\kappa T} \int_{-aY}^{aY} dy e^{-\frac{y^2}{2Y^2}} \int_0^{bR} r\, dr e^{-\frac{r^2}{2R^2}} \int_0^{2\pi} d\phi e^{-p^\mu \beta_\mu} \\ &= \frac{C_N C_0}{\kappa T} \int_{-aY}^{aY} dr_y \int_0^{bR} r\, dr\; \exp\Big(-\frac{y^2}{2Y^2} - \frac{r^2}{2R^2}\Big) \\ &\quad \times \quad e^{-\gamma p^0/T}\, e^{p_y \beta_y} \cdot 2\pi I_0\left(c_3\, r\right) \end{aligned} \quad (19)$$

Now we may use the same simplifying non-relativistic assumption as in, Eq. (5) of Ref. [26], i.e. $\gamma = 1$ is assumed, and the we approximate u^μ by v^μ as $\boldsymbol{v} = v_r \boldsymbol{e}_r + v_y \boldsymbol{e}_y + v_\phi \boldsymbol{e}_\phi = \frac{\dot{R}}{R} r \boldsymbol{e}_r + \frac{\dot{Y}}{Y} y \boldsymbol{e}_y + \omega r \boldsymbol{e}_\phi$, and thus $\gamma = 1$ is assumed, in non-relativistic approximation. It follows then:

$$\begin{aligned} A(p) &= \int dV\; n_F(p,s) \\ &= \frac{C_N C_0}{\kappa T} \quad 2\pi e^{-p^0/T} \int_{-aY}^{aY} dy \exp\Big(\frac{p_y y \dot{Y}}{TY} - \frac{y^2}{2Y^2}\Big) \\ &\quad \times \quad \int_0^{bR} r\; I_0(c_3 r) \exp\left(-\frac{r^2}{2R^2}\right) dr \\ &= \frac{C_N C_0}{\kappa T} \quad 2\pi e^{-p^0/T} \int_{-aY}^{aY} \exp\left(c_1 y - c_2 y^2\right) dy \\ &\quad \times \int_0^{bR} r\, I_0(c_3 r)\; \exp(-c_4 r^2) dr \end{aligned} \quad (20)$$

where the $c_1 = p_y \dot{Y}/(YT)$, $c_2 = 1/(2Y^2)$, $c_4 = 1/(2R^2)$ are constants.

Currently, it is assumed to be an infinite system with scaling Gaussian density profile, so that the integrals are evaluated up to infinity, i.e. the parameters $a = \infty$, $b = \infty$.

Thus, the y component integration in Eq. (21) will be calculated as:

$$\begin{aligned} &\int_{-\infty}^{+\infty} e^{c_1 y - c_2 y^2} dy \\ &= \frac{1}{2}\sqrt{\frac{\pi}{c_2}} \exp\left(\frac{c_1^2}{4c_2^2}\right)\left[\mathrm{erf}\Big(\sqrt{c_2} y - \frac{c_1}{2\sqrt{a}}\Big)\right]_{-\infty}^{+\infty} \\ &= \sqrt{\frac{\pi}{c_2}} \exp\left(\frac{c_1^2}{4c_2^2}\right), \end{aligned} \quad (21)$$

where we used the integral formula No. 2.33(1) in refer. [29]. And the error function in infinity is: $\mathrm{erf}\,(+\infty) = 1$, $\mathrm{erf}\,(-\infty) = -1$.

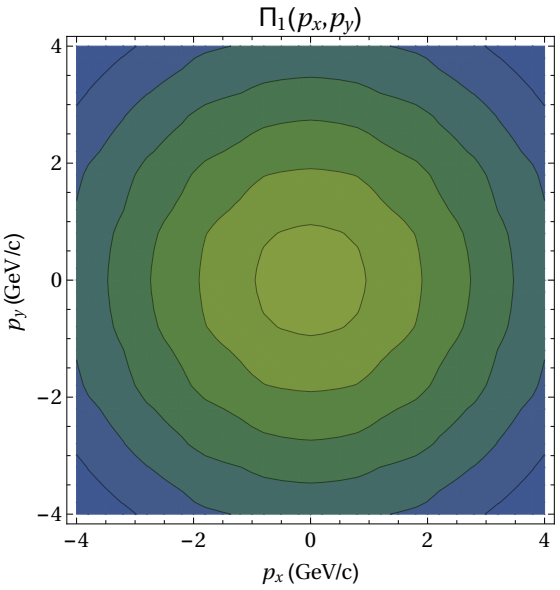

FIG. 2. (color online) The polarization of Λ particles, $\boldsymbol{\Pi}_1(\boldsymbol{p})$, in the participant Center of Mass (CM) frame for the first term containing the $(\nabla\times\boldsymbol{\beta})$-contribution, at time $t = 0.5$ fm/c after the equilibration of the rotation, in the Exact model. The polarization, $\boldsymbol{\Pi}_1(\boldsymbol{p})$, points into the $-y$-direction and changes from -1.5% at the CM-momentum ($p_x = p_y = 0$), to -8% in the corners, in 1% steps per contour line. The negative percentage indicates that the polarization is in the $-y$-direction. The structure is just like that of the energy weighted vorticity. Due to azimuthal symmetry of the Exact Model the p_x and p_z dependence of $\boldsymbol{\Pi}$ are the same.

For the integration of r component:

$$\int_0^{+\infty} r\, I_0(c_3 r)\, e^{-c_4 r^2} dr = \frac{1}{c_3\sqrt{c_4}} \exp\Big(\frac{c_3^2}{8c_4}\Big)\; M_{-\frac{1}{2},0}\Big(\frac{c_3^2}{4c_4}\Big), \tag{22}$$

where the $M_{-\mu,\nu}(z)$ is the so called 'Whittaker Function'. The integral formula used here is No.6.643(2) in refer. [29].

Now, we can write down the final integration of Eq. (21):

$$\begin{aligned} A(p) &= \int dV\; n_F(p,s) \\ &= \frac{C_N C_0}{\kappa T}\, 2\pi e^{-p^0/T} \times \sqrt{\frac{\pi}{c_2}} \exp\Big(\frac{c_1^2}{4c_2^2}\Big) \\ &\quad \times \frac{1}{c_3\sqrt{c_4}} \exp\Big(\frac{c_3^2}{4c_4}\Big)\; M_{-\frac{1}{2},0}\Big(\frac{c_3^2}{8c_4}\Big) \\ &= \frac{2\pi\sqrt{\pi}}{\kappa T} \frac{C_N C_0}{c_3\sqrt{c_2 c_4}} e^{-p^0/T} \exp\Big(\frac{c_1^2}{4c_2^2}\Big) \\ &\quad \times \exp\Big(\frac{c_3^2}{8c_4}\Big)\; M_{-\frac{1}{2},0}\Big(\frac{c_3^2}{4c_4}\Big), \end{aligned} \tag{23}$$

which is the analytical solution for the denominator of $\mathbf{\Pi}(\boldsymbol{p})$.

However, in the relativistic case, the integrations with respect to y and r can not be performed, because of the presence of $\gamma = 1/\sqrt{1 - v_r^2 - v_y^2 - v_\phi^2}$ will make integration much more involved.

B. The numerator

Ref. [26] calculates the energy weighted vorticity, which is azimuthally symmetric, i.e. independent of the azimuthal angle ϕ. In the definition of the polarization, Eq. (7), we have $p^0\, n_F(p,x) = \epsilon\, n_F(p,x)$ for Λs with momentum p. In [26], however, the energy weighting is performed with the total energy density of the fluid $E_{tot} = E_{int} + E_{kin}$, which in general is not the same as $\epsilon\, n_F(p,x)$. On the other hand the bare vorticity is just a constant in the non-relativistic exact model, while the EoS may be more general and it may lead to more involved $R(t)$ and $Y(t)$ dependence than the ideal Jüttner gas approximation would allow.

Thus we use the direct non-relativistic vorticity values from Ref. [26], and not the presented energy weighted vorticity, i.e.

$$\boldsymbol{\nabla} \times \boldsymbol{\beta} = -2\omega \boldsymbol{e}_y / T\ , \tag{24}$$

so that the vorticity has only y-directed component in the Exact model. This will make the numerator simple:

$$\begin{aligned} B(p) &\equiv \int dV\, n_F\big(\nabla \times \beta\big) \\ &= \int_0^R r\, dr \int_{-Y}^{+Y} dy \int_0^{2\pi} d\phi\; n_F(x,p)\big(\frac{-2\omega \boldsymbol{e}_y}{T}\big)\ . \\ &= \frac{-2\omega \boldsymbol{e}_y}{T} \int_0^R r\, dr \int_{-Y}^{+Y} dy \int_0^{2\pi} d\phi\; n_F(x,p) \\ &= \frac{-2\omega \boldsymbol{e}_y}{T} \times A(p) \end{aligned} \tag{25}$$

Therefore, the first term of polarization vector, i.e. Eq. (7) will be:

$$\begin{aligned} \mathbf{\Pi}_1(p) &= -\frac{\hbar\epsilon}{8m} \frac{\int dV n_F(x,p)\, (\nabla \times \boldsymbol{\beta})}{\int dV n_F(x,p)} \\ &= \frac{\hbar\epsilon\omega}{4mT} \boldsymbol{e}_y\ , \end{aligned} \tag{26}$$

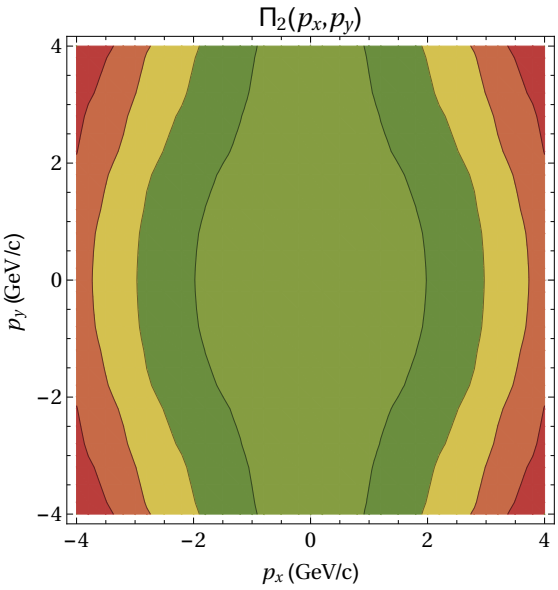

FIG. 3. (color online) The absolute value of Λ-polarization, $\mathbf{\Pi}_2(\boldsymbol{p})$, in the participant Center of Mass (CM) frame for the second term containing the $(\partial_t \boldsymbol{\beta})$-contribution, at time $t = 0.5$ fm/c after the equilibration of the rotation, in the Exact model. The polarization changes from zero at the CM-momentum ($p_x = p_y = 0$), up to 20% in the corners at $p_x = -4$GeV/c, in 2.5% steps per contour line. In the corners at $p_x = 4$GeV/c, the polarization is 12%. This second term is orthogonal to $\boldsymbol{p}$, and it is smaller, especially at CM-momenta, where it is negligible. This term arises from the expansion, which is increasing rapidly in the Exact model with time and also increases with the radius. At large radius the larger expansion leads to larger momenta. The structure of the 2nd component of polarization arises from the asymmetries of the different components of $\mathbf{\Pi}_2(\boldsymbol{p})$

which means the polarization vector arising from the vorticity, $\mathbf{\Pi}_1(p)$, in the exact rotation model is a constant, (although time dependent), and parallel to the y-axis. At the same time, $\Pi_0(p)$ shows a p dependence according to Eq. (6).

One may add the Freeze-Out (FO) probability to the integral. According to the Ref. [30], the FO probability is $w_s = (p_\mu\, \hat{\sigma}^\mu_s)\ (\boldsymbol{p}\cdot\boldsymbol{u}(x))$, where the approximation is used that the FO direction, $\hat{\sigma}^\mu_s$ is parallel to the flow velocity, $\boldsymbol{u}(x) = \gamma \boldsymbol{v}(x)$. In the first term of the nominator, which depends on the constant y-directed vorticity this FO probability influences the nominator and denominator the same way, so the effect of the two integrals cancel each other with the FO probability also.

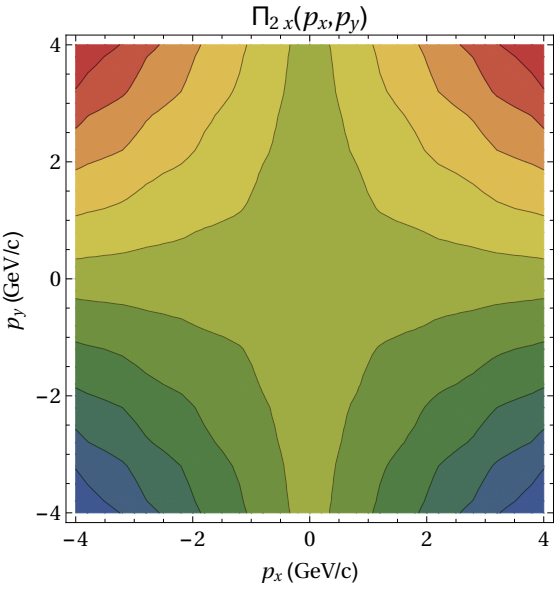

FIG. 4. (color online) The x component of the Λ-polarization, $\mathbf{\Pi}_{2x}(\boldsymbol{p})$, in the participant Center of Mass (CM) frame for the second term containing the $(\partial_t\boldsymbol{\beta})$-contribution, at time $t = 0.5$ fm/c after the equilibration of the rotation, in the Exact model. The polarization vanishes at the CM-momentum ($p_x = p_y = 0$), and changes from zero up/down to $\pm 8\%$ in the corners, in 1% steps per contour line. This term arises from the expansion, which is increasing rapidly in the Exact model with time and also increases with the radius. At large radius the larger expansion leads to larger momenta.

C. The second term

The numerator in second term of polarization vector reads:

$$\boldsymbol{C}(\boldsymbol{p}) \equiv \int dV n_F(x,p)\,(\partial_t\boldsymbol{\beta} + \boldsymbol{\nabla}\beta^0)\ . \tag{27}$$

If, in the non-relativistic limit, $\gamma = 1$ is assumed, then $\nabla\beta^0 = 0$, and $\partial_t\beta = \partial_t(\boldsymbol{v}/T)$, so we have to evaluate only the first term of the sum in the integrand. According to Ref. [26, 31], the time derivatives of velocity are:

$$\begin{aligned}
\partial_t v_r &= \left[\left(\frac{\ddot{R}}{R} - \frac{\dot{R}^2}{R^2}\right) - \omega^2\right] r \equiv c_5 r \\
\partial_t v_\phi &= \left(\dot{\omega} + 2\frac{\dot{R}}{R}\omega\right) r \equiv c_6 r \\
\partial_t v_y &= \left[\frac{\ddot{Y}}{Y} - \frac{\dot{Y}^2}{Y^2}\right] y \equiv c_7 y\ ,
\end{aligned} \tag{28}$$

where $c_5 = (\ddot{R}/R - \dot{R}^2/R^2 - \omega^2)$, $c_6 = (\dot{\omega} + 2(\dot{R}/R)\omega)$, and $c_7 = (\ddot{Y}/Y - \dot{Y}^2/Y^2)$. Therefore,

$$\partial_t\boldsymbol{\beta} = \big(c_5 r\boldsymbol{e}_r + c_6 r\boldsymbol{e}_\phi + c_7 y\boldsymbol{e}_y\big)/T.$$

Eq. (27) is a volume integral of a vectorial quantity, which is not convenient perform in cylindrical coordinates, so we transform it into Cartesian coordinates: $\boldsymbol{e}_r = \cos\phi\,\boldsymbol{e}_x + \sin\phi\,\boldsymbol{e}_z$, $\boldsymbol{e}_\phi = -\sin\phi\,\boldsymbol{e}_x + \cos\phi\,\boldsymbol{e}_z$. Therefore,

$$\begin{aligned}
&T\cdot\partial_t\boldsymbol{\beta} \\
&= c_5 r\cos\phi\boldsymbol{e}_x + c_5 r\sin\phi\,\boldsymbol{e}_z \\
&\quad -c_6 r\sin\phi\boldsymbol{e}_x + c_6 r\cos\phi\,\boldsymbol{e}_z + c_7 y\,\boldsymbol{e}_y \\
&= \big(c_5\cos\phi - c_6\sin\phi\big) r\,\boldsymbol{e}_x \\
&\quad + \big(c_5\sin\phi + c_6\cos\phi\big) r\,\boldsymbol{e}_z + c_7 y\,\boldsymbol{e}_y\ .
\end{aligned} \tag{29}$$

The integral of Eq. (27) can be expanded as:

$$\begin{aligned}
\boldsymbol{C}(\boldsymbol{p}) &= \int dV n_F(x,p)\,\partial_t\boldsymbol{\beta} \\
&= \frac{C_N C_0}{\kappa T} e^{-p_0/T} \iiint r dr d\phi dy\, \exp\left(c_1 y - c_2 y^2\right) \\
&\qquad \times \exp\left(a\cos\phi - b\sin\phi - c_4 r^2\right)\partial_t\boldsymbol{\beta}\ ,
\end{aligned} \tag{30}$$

where a and b are defined after Eq. (17).

It is convenient to define an integrating operator, based on integration $A(\boldsymbol{p})$:

$$\begin{aligned}
\bar{A} &= \int dV n_F(x,p)\ \times \\
&= \iiint r\,dr\,d\phi\,dy\, e^{c_1 y - c_2 y^2} e^{a\cos\phi - b\cos\phi - c_4 r^2} \times\ ,
\end{aligned}$$

and then Eq. (30) will be:

$$\begin{aligned}
\boldsymbol{C}(\boldsymbol{p}) &= \bar{A}\cdot\partial_t\boldsymbol{\beta} \\
&= \bar{A}\cdot\frac{1}{T}\big(c_5\cos\phi - c_6\sin\phi\big) r\,\boldsymbol{e}_x \\
&\quad + \bar{A}\cdot\frac{1}{T}\big(c_5\sin\phi + c_6\cos\phi\big) r\,\boldsymbol{e}_z \\
&\quad + \bar{A}\cdot\frac{1}{T} c_7 y\,\boldsymbol{e}_y \\
&\equiv \frac{1}{T}\left(I\boldsymbol{e}_x + J\boldsymbol{e}_z + H\boldsymbol{e}_y\right)\ ,
\end{aligned} \tag{31}$$

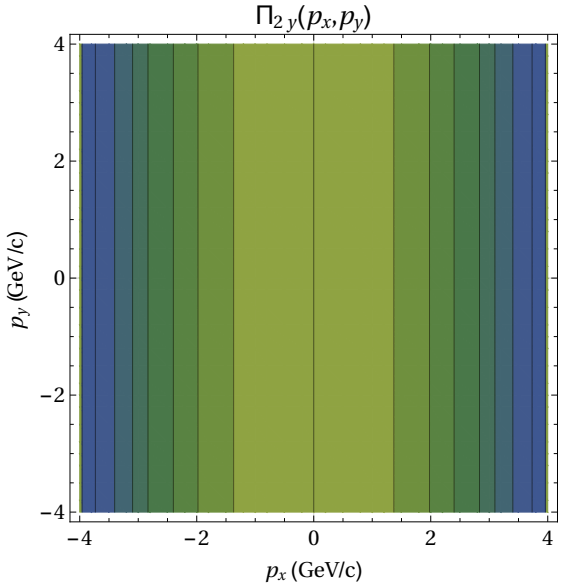

FIG. 5. (color online) The y-component of Λ-polarization, $\mathbf{\Pi}_2(\boldsymbol{p})$, in the participant Center of Mass (CM) frame for the first term containing the $(\partial_t\boldsymbol{\beta})$-contribution, at time $t = 0.5$ fm/c after the equilibration of the rotation, in the Exact model. The polarization changes from zero in the middle to -8% at $p_x = \pm 4$GeV/c, in 1% steps per contour line. This y-component points into the axis-direction just as the first term, $\mathbf{\Pi}_1$, thus these two are additive. The y-component of $\mathbf{\Pi}_2(\boldsymbol{p})$ does not depend of p_y, as shown in Eq. (40).

where we defined:

$$
\begin{aligned}
I &\equiv \bar{A}\cdot\big(c_5\cos\phi - c_6\sin\phi\big)r\ ,\\
J &\equiv \bar{A}\cdot\big(c_5\sin\phi + c_6\cos\phi\big)r\ ,\\
H &\equiv \bar{A}\cdot c_7 y\ .
\end{aligned}
$$

H can be expanded as:

$$
\begin{aligned}
H &= \bar{A}\cdot c_7 y\\
&= \frac{C_N C_0}{\kappa T} e^{-p_0/T}\int dy\, c_7\, y\exp\big(c_1 y - c_2 y\big)\\
&\quad\times\iint r dr\, d\phi\,\exp\Big[(a\cos\phi - b\sin\phi) - c_4 r^2\Big]\ .
\end{aligned}
\tag{32}
$$

According to Eqs. (18) and (22), the integral with respect to r and ϕ is:

$$
\begin{aligned}
&\iint r dr\, d\phi\,\exp\Big[(a\cos\phi - b\sin\phi) - c_4 r^2\Big]\\
&=\frac{2\pi}{c_3\sqrt{c_4}}\exp\Big(\frac{c_3^2}{8c_4}\Big)\ M_{-\frac{1}{2},0}\Big(\frac{c_3^2}{4c_4}\Big)\ ,
\end{aligned}
$$

and the integral with respect to y is calculated as:

$$
\int dy\, c_7\, y\exp\big(c_1 y - c_2 y^2\big) = \frac{c_7 c_2}{2c_2}\sqrt{\frac{\pi}{c_2}}\exp\Big(\frac{c_1^2}{4c_2^2}\Big)\ ,
$$

where we used the integral formula No. 2.33(6) in Ref. [29]. Therefore, Eq. (32) becomes:

$$
\begin{aligned}
H =&\frac{2\pi\sqrt{\pi}C_N C_0}{\kappa T}e^{-p_0/T}\frac{c_7 c_1}{2c_3 c_2\sqrt{c_4 c_2}}\\
&\times\exp\Big(\frac{c_3^2}{8c_4}\Big)\exp\Big(\frac{c_1^2}{4c_2^2}\Big)M_{-\frac{1}{2},0}\Big(\frac{c_3^2}{4c_4}\Big)\ .
\end{aligned}
\tag{33}
$$

I can be expanded as:

$$
\begin{aligned}
I &= \bar{A}\cdot\Big(c_5\cos\phi - c_6\sin\phi\Big)r\\
&= \frac{C_N C_0}{\kappa T}e^{-p_0/T}\int dy\exp\big(c_1 y - c_2 y^2\big)\int dr\, r^2 e^{-c_4 r^2}\\
&\quad\times\int d\phi\exp\Big[a\cos\phi - b\sin\phi\Big]\Big(c_5\cos\phi - c_6\sin\phi\Big)\ ,
\end{aligned}
\tag{34}
$$

According to Eqs. No. 3.937 (1) and (2) in Ref. [29], one can first perform the integration with respect to ϕ:

$$
\begin{aligned}
&\int_0^{2\pi} d\phi\exp\Big[a\cos\phi - b\sin\phi\Big]\Big(c_5\cos\phi - c_6\sin\phi\Big)\\
&= \frac{c_8}{c_3}2\pi I_1(c_3 r)\ ,
\end{aligned}
$$

where $c_8 = (c_5 a' - c_6 b')$, and $a' = a/r = |p_x|\dot{R}/TR$, $b' = b/r = |p_x|\omega/T$. Then, the integral with respect to r becomes:

$$
\begin{aligned}
&\int_0^\infty dr r^2 e^{-c_4 r^2}\cdot\frac{c_8}{c_3}2\pi I_1(c_3 r)\\
&= 2\pi\frac{c_8}{c_3}\int_0^\infty dr r^2 I_1(c_3 r)e^{-c_4 r^2}\\
&= 2\pi\frac{c_8}{c_3^2 c_4}\exp\Big(\frac{c_3^2}{8c_4}\Big)M_{-1,\frac{1}{2}}\Big(\frac{c_3^2}{4c_4}\Big)\ ,
\end{aligned}
\tag{35}
$$

where we used the 6.643(2) of Ref. [29]. The integration with respect to y here is separable and is the same as Eq. (21). So, substituting Eqs. (36) and (21) into I, i.e. Eq. (34), one obtains:

$$
\begin{aligned}
I =&\frac{2\pi\sqrt{\pi}C_N C_0}{\kappa T}e^{-p_0/T}\frac{c_8}{c_3^2 c_4\sqrt{c_2}}\\
&\times\exp\Big(\frac{c_3^2}{8c_4}\Big)\exp\Big(\frac{c_1^2}{4c_2^2}\Big)M_{-1,\frac{1}{2}}\Big(\frac{c_3^2}{4c_4}\Big)\ .
\end{aligned}
\tag{36}
$$

Evaluating the integral J is similar to I:

$$
\begin{aligned}
J =&\frac{2\pi\sqrt{\pi}C_N C_0}{\kappa T}e^{-p_0/T}\frac{c_9}{c_3^2 c_4\sqrt{c_2}}\\
&\times\exp\Big(\frac{c_3^2}{8c_4}\Big)\exp\Big(\frac{c_1^2}{4c_2^2}\Big)M_{-1,\frac{1}{2}}\Big(\frac{c_3^2}{4c_4}\Big)\ .
\end{aligned}
\tag{37}
$$

where the only difference is: $c_9 = (c_5 b' + c_6 a')$ compared to c_8 in I.

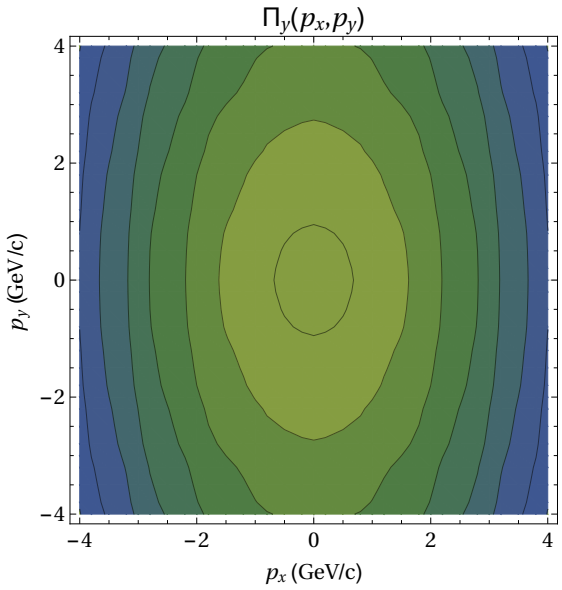

FIG. 6. (color online) The y-component of Λ-polarization, $\mathbf{\Pi}(\boldsymbol{p})$, in the participant Center of Mass (CM) frame for the second term containing the $(\partial_t\boldsymbol{\beta})$-contribution, at time $t = 0.5$ fm/c after the equilibration of the rotation, in the Exact model. The polarization is -1.5% at the CM-momentum ($p_x = p_y = 0$), it is -16% in the corners. The change is in steps of 2% per contour line.

Then, substituting I, J, H back into Eq. (31), one can obtain the analytical solution for numerator in second term of polarization vector as:

$$\begin{aligned}
&\boldsymbol{C}(\boldsymbol{p}) = \int dV n_F(x,p)\,\partial_t\boldsymbol{\beta} \\
&= \frac{1}{T}\left(I\boldsymbol{e}_x + J\boldsymbol{e}_z + H\boldsymbol{e}_y\right) \\
&= \frac{2\pi\sqrt{\pi}C_N C_0}{\kappa T^2} e^{-p_0/T}\exp\left(\frac{c_3^2}{8c_4}\right)\exp\left(\frac{c_1^2}{4c_2^2}\right)\times \\
&\left[\frac{c_8}{c_3^2 c_4\sqrt{c_2}} M_{-1,\frac{1}{2}}\left(\frac{c_3^2}{4c_4}\right)\boldsymbol{e}_x + \frac{c_9}{c_3^2 c_4\sqrt{c_2}} M_{-1,\frac{1}{2}}\left(\frac{c_3^2}{4c_4}\right)\boldsymbol{e}_z\right. \\
&\left. + \frac{c_7 c_1}{2c_3 c_2\sqrt{c_4 c_2}} M_{-\frac{1}{2},0}\left(\frac{c_3^2}{4c_4}\right)\boldsymbol{e}_y\right] .
\end{aligned} \tag{38}$$

Dividing this by $A(\boldsymbol{p})$, i.e. Eq. (23), one gets:

$$\frac{\boldsymbol{C}(\boldsymbol{p})}{A(\boldsymbol{p})} = \frac{1}{T}\left[\frac{c_8}{c_3\sqrt{c_4}}\frac{M_{-1,\frac{1}{2}}}{M_{-\frac{1}{2},0}}\boldsymbol{e}_x + \frac{c_9}{c_3\sqrt{c_4}}\frac{M_{-1,\frac{1}{2}}}{M_{-\frac{1}{2},0}}\boldsymbol{e}_z + \frac{c_7 c_1}{2c_2}\boldsymbol{e}_y\right]. \tag{39}$$

Then, we obtain the second term of polarization vector:

$$\begin{aligned}
\mathbf{\Pi}_2(\boldsymbol{p}) =& \frac{\hbar\boldsymbol{p}}{8m}\times\frac{\boldsymbol{C}(\boldsymbol{p})}{A(\boldsymbol{p})} \\
=& \frac{\hbar}{8mT}\left[\frac{p_y c_9}{c_3\sqrt{c_4}}\frac{M_{-1,\frac{1}{2}}}{M_{-\frac{1}{2},0}}\boldsymbol{e}_x - \frac{|p_x|c_9}{c_3\sqrt{c_4}}\frac{M_{-1,\frac{1}{2}}}{M_{-\frac{1}{2},0}}\boldsymbol{e}_y\right. \\
&+ \left.\left(\frac{|p_x|c_7 c_1}{2c_2} - \frac{p_y c_8}{c_3\sqrt{c_4}}\frac{M_{-1,\frac{1}{2}}}{M_{-\frac{1}{2},0}}\right)\boldsymbol{e}_z\right].
\end{aligned} \tag{40}$$

As we can see, and it is given also by the definition, Eq. (7), the second therm of polarization is orthogonal to the particle momentum:

$$\mathbf{\Pi}_2(\boldsymbol{p}) \;\perp\; \boldsymbol{p}\,, \tag{41}$$

thus if we use the choice that $\boldsymbol{p}$ should be in the $[x,y]$-plane and its z-component should vanish, then in $\mathbf{\Pi}_2(\boldsymbol{p})$ the y-component p_x only, see Fig. 5.

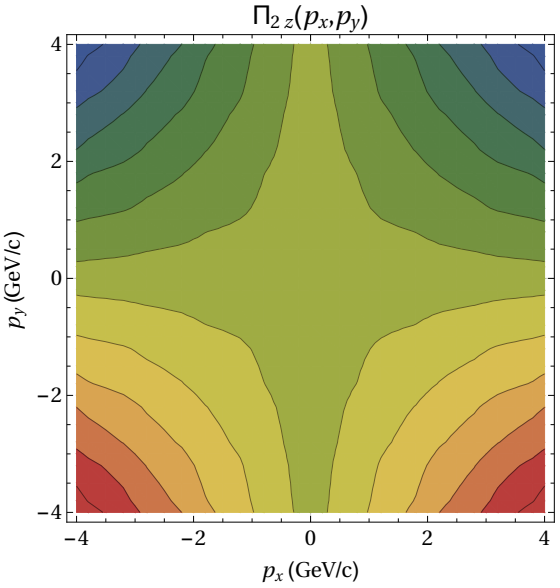

FIG. 7. (color online) The z-component of Λ-polarization, $\mathbf{\Pi}_2(\boldsymbol{p})$, in the participant Center of Mass (CM) frame for the second term containing the $(\partial_t\boldsymbol{\beta})$-contribution, at time $t = 0.5$ fm/c after the equilibration of the rotation, in the Exact model. The polarization vanishes at the CM-momentum ($p_x = p_y = 0$), it is $\pm 3\%$ in the corners. The change is in steps of 0.5% per contour line. The corners at $p_y = -4$GeV/c are positive while at $p_y = 4$GeV/c are negative.

D. Conclusion

Finally, adding Eqs. (40) and (26) we get the analytical solution for Λ-polarization in the Exact model:

$$\mathbf{\Pi}(p) = \frac{\hbar}{8mT}\left[\frac{p_y c_9}{c_3\sqrt{c_4}}\frac{M_{-1,\frac{1}{2}}}{M_{-\frac{1}{2},0}}\boldsymbol{e}_x + \Big(2\epsilon\omega - \frac{|p_x|c_9}{c_3\sqrt{c_4}} \times \frac{M_{-1,\frac{1}{2}}}{M_{-\frac{1}{2},0}}\Big)\boldsymbol{e}_y + \Big(\frac{|p_x|c_7c_1}{2c_2} - \frac{p_y c_8}{c_3\sqrt{c_4}}\frac{M_{-1,\frac{1}{2}}}{M_{-\frac{1}{2},0}}\Big)\boldsymbol{e}_z\right]. \tag{42}$$

Notice that Eq. (42) is the analytical solution in the non-relativistic limit. The 'Whittaker Function', $M_{\mu,\nu}(z)$, is the confluent hypergeometric function. For the relativistic case, the integrations of the Λ-polarization vector can not be performed analytically, because of the presence of $\gamma = 1/\sqrt{1-v_r^2-v_y^2-v_\phi^2}$, which will make the integrations more involved. Thus, a numerical solution for the Λ-polarization would be needed.

The effect of vorticity is shown in Fig. 2. The non-relativistic Exact model can handle reactions with modest energy and modest rotation, so the overall vorticity and the resulting polarization is not too large. Furthermore the rotation and vorticity decrease with time while the radial and axial expansion increases. This expansion leads to the second term of polarization, $\mathbf{\Pi}_2$, which depends on $\partial_t\boldsymbol{\beta}$ (while the $\boldsymbol{\nabla}\beta^0$ terms vanishes in the non-relativistic approximation). Thus this second term is of comparable magnitude to the term arising from local vorticity. See Fig. 3.

The presented plots are such that p_x points into the direction of the observed Λ-particle, while the p_y is the axis direction. All results should be either symmetric or antisymmetric for a $\pm p_y$ change. On the other hand reversing the p_x axis must not change the data, as the x-axis is chosen to be the direction of the argument of $\mathbf{\Pi}(\boldsymbol{p})$, which must be azimuthally symmetric in the $[x, y]$-plane.

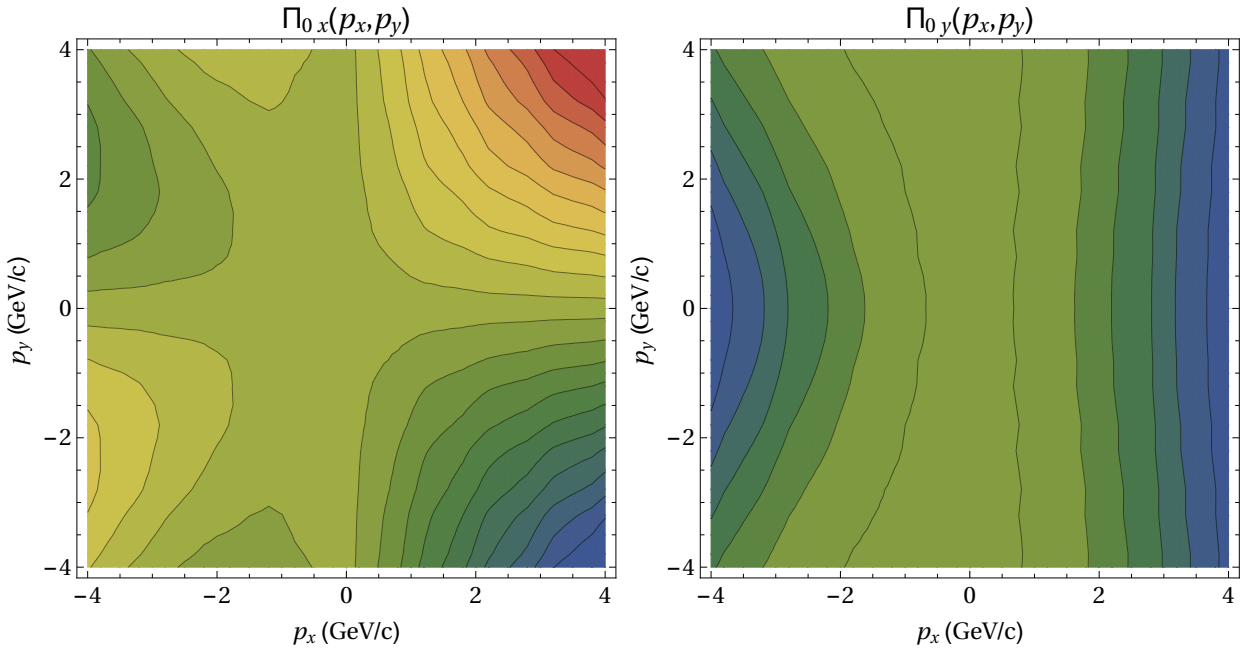

FIG. 8. (color online) The radial, x, and axial, y, components of Λ-polarization, $\mathbf{\Pi}_0(\boldsymbol{p})$, in the Λ's rest frame. For $\Pi_{0x}(\boldsymbol{p})$ the contours represent changes of 1% from −9.5% in the upper left-hand corner to 9.5% in the upper right-hand corner, whereas the contours of $\Pi_{0y}(\boldsymbol{p})$ change in steps of 2% ranging from $\Pi_{0y} = 0$ (!) at the CM momentum ($p_x = p_y = 0$) to −12% for $p_x = \pm 4$GeV/c at the edges. Both plots are asymmetric due to the Lorentz boost to the Λ rest frame.

The polarization arising from the dynamics of the radial and spherical expansion, $\mathbf{\Pi}_2$, was not discussed before in the literature, as the dominance of the vorticity effect was anticipated and studied up to now. The $\mathbf{\Pi}_2$ plots in Figs. 3, 4, 5, 7, show the components of the polarization arising from the dynamics of the spherical expansion. The most interesting y-component arises from the x-component of the momentum ans the z-component

of the thermal velocity change $\dot{\beta}_z$ (Fig. 5).

Now if we study the axis directed components, this is given by $\Pi_y = \Pi_{1y} + \Pi_{2y}$. Both these terms have a negative maxima of the same magnitude, -8%, at the corners, $p_x, p_y = \pm 4\mathrm{GeV/c}$, thus these terms add up constructively and result in Λ-particle polarizations reaching -16% at high momenta. At small momenta the polarization is still the same sign but has a reduced value of the order of 1.5% arising from the vorticity (Fig. 6).

In this Exact model the x and z components of the polarization arise only from the second term, $\mathbf{\Pi}_2(\boldsymbol{p})$. The x component is reaching $\pm 8\%$, while the z component is smaller, it reaches about $\pm 3\%$. These both are asymmetric for $\pm p_y$ change, and show an opposite symmetry. The x-component is proportional to p_y and the dynamics of radial expansion, thus it follows the signature of p_y, Fig. 4. The z-component is proportional to p_y and the dynamics of radial expansion, thus it follows the signature of p_y, Fig. 7. The z-component is proportional to $p_x\dot{\beta}_y$ and inversely proportional to $p_y\dot{\beta}_x$, Fig. 7. These two effects compensate each other so the maxima of the polarization are smaller and the symmetry is opposite to that of the x-component. This term is sensitive to the balance between the axial expansion and the radial expansion in the model.

The Λ polarization is measured via the angular distribution of the decay protons in the Λ's rest frame, as shown in Eq. 6. The resulting distribution is shown in Fig. 8. This new studies indicate that the dynamics of the expansion may lead to non-negligible contribution to the observable polarization. The structure of $\Pi_{0y}(\boldsymbol{p})$ is similar to the one obtained in Ref. [28], but here the contribution of the "second", $\partial_t\boldsymbol{\beta}$ term is also included, which makes the y-directed polarization stronger at high p_x values, 12%, while it was 9% in Ref. [28], both in the negative y-direction. Furthermore, the second term changes the structure, of the momentum dependence of $\Pi_{0y}(\boldsymbol{p})$, and it becomes $\pm p_x$ asymmetric.

Recently the vorticity and polarization were also studied in two fluid dynamical models [32]. The initial states that were used from Bozek and Gubser neglected fully the initial shear flow in the central domain of the reaction, in contrast to other models where this is present [1, 2, 21, 33]. This results in negligible thermal vorticity in the central domain of the collision (Figs. 3, 13 of Ref. [32]), and consequently a negligible polarization from the vorticity from the "first term" discussed here. Thus, the observed vorticity arises from the "second term". In this work we analyzed and compared the two terms, and the Exact model, – including both rotation and expansion, and vorticity arising from both effects – , enables us to study the consequences of the two terms separately. This study indicates that the assumptions regarding the initial state are influencing the predictions on the observed vorticity, while in all cases observable polarization is predicted.

ACKNOWLEDGEMENTS

Enlightening discussions with Sharareh Mehrabi Pari, Francesco Becattini, Eirik Hatlen, and Sindre Velle are gratefully acknowledged. One of the authors, Y.L.X., is supported by the China Scholarship Council.

[1] V.K. Magas, L.P. Csernai, and D.D. Strottman, *Phys. Rev.* C **64** 014901 (2001).
[2] V.K. Magas, L.P. Csernai, and D.D. Strottman, *Nucl. Phys.* A **712** 167 (2002).
[3] F. Gelis, arXiv:1312.5497v2 [hep-ph] (2013).
[4] B. Alver, M. Baker, C. Loizides, P. Steinberg, arXiv:0805.4411v1 [nucl-ex] (2008).
[5] Brett McInnes and Edward Teo, Nucl. Phys. B **878**, 186 (2014).
[6] Brett McInnes, arXiv: 1403.3258v1 [hep-th].
[7] L.P. Csernai, W. Greiner, H. Stöcker, I.Tanihata, S. Nagamiya, J. Knoll, *Phys. Rev.* **C25**, 2482 (1982).
[8] L.P. Csernai, G. Fai, J. Randrup, Phys. Lett. B **140**, 149 (1984).
[9] L.P. Csernai, V.K. Magas, H. Stöcker, and D.D. Strottman, Phys. Rev. C **84**, 024914 (2011).
[10] L.P. Csernai, D.D. Strottman and Cs. Anderlik, Phys. Rev. C **85**, 054901 (2012).
[11] Y.B. Ivanov, A.A. Soldatov, Phys. Rev. C **91**, 024915 (2015).
[12] Y.B. Ivanov, A.A. Soldatov, Phys. Rev. C **91**, 024915 (2015), arXiv: 1412.1669v2 [nucl-th] (2015)
[13] H.W. Barz, B. Kämpfer, L.P. Csernai, B. Lukács Phys. Lett. B **143**, 334 (1985).
[14] Csernai, L. P., and S. Velle, arXiv:1305.0385 (2013).
[15] R. Hanbury Brown and R.Q. Twiss, Phil. Mag. 45, 663 (1954); and R. Hanbury Brown and R.Q. Twiss, Nature, 178, 1046 (1956).
[16] M.I. Gorenstein, M. Hauer, O.N. Moroz, Phys. Rev. C **77**, 024911 (2008), arXiv: 0708.0138v1 [nucl-th] (2007).
[17] L.P. Csernai, J.I. Kapusta, L.D. McLerran, Phys. Rev. Lett. **97**, 152303 (2006).
[18] L.P. Csernai, V.K. Magas, D.J. Wang, Phys. Rev. C **87**, 034906 (2013).
[19] D.J. Wang, Z. Néda, and L.P. Csernai, Phys. Rev. C **87**, 024908 (2013).
[20] L.P. Csernai, D.J. Wang, and T. Csörgő, Phys. Rev. C **90**, 024901 (2014).
[21] G. Graef, M. Bleicher, M. Lisa, Phys. Rev. C **89**, 014903 (2014).
[22] A. Repko, P.G. Reinhard, V.O. Nesterenko, and J. Kvasil, Phys. Rev. C **87**, 024305 (2013).
[23] W. Zuo, S.X. Gan, U. Lombardo, Chin. Phys. C **36** (2012) 967, arXiv:1310.1388v1 [nucl-th]
[24] P.G. Reinhard, V.O. Nesterenko, A. Repko, and J. Kvasil, Phys. Rev. C **89**, 024321 (2014).
[25] T. Csörgő, M.I. Nagy, Phys. Rev. C **89**, 044901 (2014).

[26] L.P. Csernai, J.H. Inderhaug, Int. J. Modern Physics E **24**, 1550013 (2015), arXiv:1503.03247v1 [nucl-th]
[27] F. Becatinni, V. Chandra, L. Del Zanna, E. Grossi, Annals of Physics **338**, 32 (2013).
[28] F. Becattini, L.P. Csernai, and D.J. Wang, Phys. Rev. C **88**, 034905 (2013).
[29] Jeffrey, Alan, and Daniel Zwillinger, eds.: Table of integrals, series, and products. Academic Press, 2007.
[30] L.P. Csernai, S. Velle, D.J. Wang, Phys. Rev. C **89**, 034916 (2014).
[31] Horst Stöcker: *Taschenbuch Der Physik*, (Harri Deutsch, 2000), 1.3.2/6d.
[32] F. Becattini, G. Inghirami, V. Rolando, A. Beraudo, L. Del Zanna, A. De Pace, M. Nardi, G. Pagliara, and V. Chandra, arXiv:1501.04468v2 [nucl-th] (2015).
[33] Guangyao Chen, Rainer J. Fries Phys. Lett. B **723** 417 (2013).

Chapter 5

Conclusion

In peripheral heavy ion collisions, there is substantial angular momentum in the initial state, giving rise to rotation and vorticious flow. Due to the small ratio of η/s of hot and dense nuclear matter, turbulent phenomena may occur to further enhance rotation in the QGP phase. When the system cools and expands, it slows, due to the transfer of energy to expansion. Hence, we use an exact analytical, self-similar rotating fluid dynamical model which may accommodate the slowing of rotation. In this model we explored the transverse polarization of Λ's in the non-relativistic case.

In this scenario, we have discussed the transverse polarization of Λ's in peripheral heavy ion collisions. Provided spin degrees of freedom locally equilibrate, polarization of secondary hyperons occur via a thermomechanical effect (due to equipartioning of energy from spin degrees of freedom). This leads to aligned spin for hyperon and antihyperon alike. We measure the polarization using the azimuthal distribution of decay protons, hence we expect the strongest polarization for Λ with momenta in the reaction plane. The polarization points in the negative y-direction, and arises from the four-gradient, temporal derivative, and curl of the inverse temperature field which we saw amounted to about 9%, assuming that only the curl of the inverse temperature field was to contribute significantly. It vanishes for center of mass transverse momenta $p_x = 0$ and $p_y = 0$. The p_x dependence was strong for fixed p_y, while a change in p_y would yield somewhat less rapid increase. The largest transverse polarization was measured with $p_x = \pm 4$ GeV/c in the center of mass system, which gave 16%.

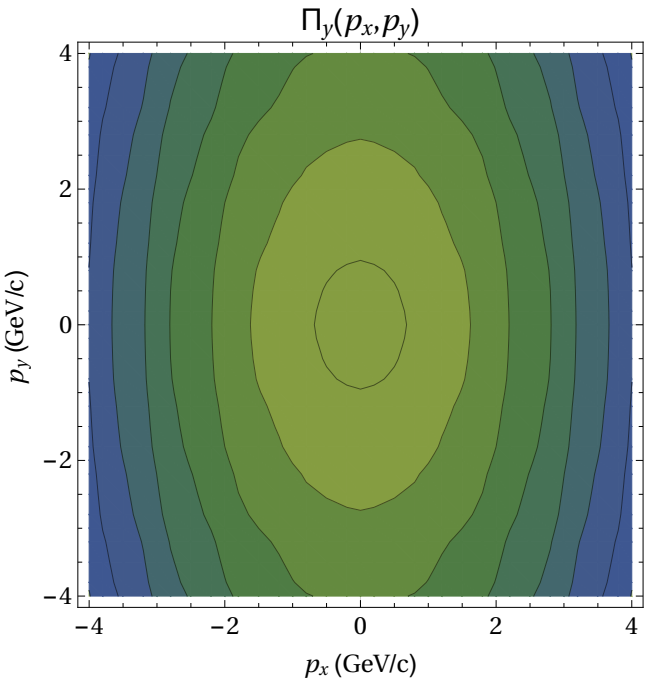

Figure 5.1: The y-component of the polarization 4.5 fm/c after the initiation of the fluid dynamical model (0.5 fm/c after initiation of the exact model). For center of mass transverse momenta $p_x = p_y = 0$ the polarization is 1% and it increases in 1.5% steps per contour line to 16% for large transverse momenta.

Here we have shown that assuming the gradient of the inverse temperature is negligible was mistaken. It should be noted that our calculating the terms was a matter of "confirming" their insignificance, so we were surprised as well. This is promising with respect to performing a measurement; but we should still try to maximize, which now seems a more complicated task, given that the radial and axial part do not vanish as we expected.

Bibliography

[1] Y. Xie, R.C. Glastad, L.P. Csernai, arXiv:1505.07221v1 [nucl-th]

[2] S. Z. Belen'kji, L. D. Landau, Il Nuovo Cimento, 3(1) Supplement, 15-31

[3] R. C. Hwa, Phys. Rev. D 10, 2260 (1974)

[4] J. D. Bjorken, Phys. Rev. D 27, 140 (1983)

[5] T. Csörgö, ActaPhys.Polon.B37:483-494 (2006) arXiv:hep-ph/0111139v2

[6] T. Csörgö, M. I. Nagy, M. Csanád, J. Phys. G35: 104128,2008 arXiv:0805.1562v1 [nucl-th]

[7] M. I. Nagy, Phys.Rev.C83:054901 (2011) arXiv:0909.4285v2 [nucl-th]

[8] T. Hirano, M. Gyulassy, Nucl. Phys. A769:71-94 (2006), arXiv:nucl-th/0506049v2

[9] SQ. Feng, Y. Zhong, Physical Review C 83, 034908 (2011) arXiv:1202.2195v1 [hep-ph]

[10] W. Israela, J.M. Stewart, Annals of Physics, 118(2), 341–372 (1979)

[11] Harri Niemi, "Collective dynamics in relativistic nuclear collisions", Nuclear Physics A, Volume 931, November 2014, Pages 227–237

[12] M.G. Alford, A. Schmitt, K. Rajagopal, T. Schäfer, Rev. Mod. Phys. **80**, 1455, 2008

[13] PHENIX Collaboration, K. Adcox, *et al.*, Nucl. Phys. A757: 184-283, 2005, arXiv:nucl-ex/0410003v3

[14] P. K. Kovtun, D.T. Son, A.O. Starinets, Phys. Rev. Lett. **94**, 111601 (2005)

[15] GY Qin, H. Petersen, S.A. Bass, B. Müller, Phys. Rev. C **82**, 064903 – Published 13 December 2010

[16] S. Floerchinger, U.A. Wiedemann, Phys. Rev. C 88, 044906 (2013) arXiv:1307.7611v1 [hep-ph]

[17] M. Luzum, P. Romatschke, Phys. Rev. C 78, 034915 – Published 26 September 2008; Erratum Phys. Rev. C 79, 039903 (2009)

[18] O.V. Rogachevsky, A.S. Sorin, O.V. Teryaev, Phys. Rev. C **82**, 054910 (2010)

[19] O.V. Teryaev, Physics of Atomic Nuclei, 2012, Vol. 75, No. 6, pp. 748–752.

[20] J. Berges, K. Boguslavski, S. Schlichting, R.Venugopalan, Phys. Rev. D **89**, 074011 (2014) arXiv:1303.5650v2 [hep-ph]

[21] J. Berges, b, B. Schenke, S. Schlichting, R. Venugopalan, Nuclear Physics A, Volume 931, November 2014, Pages 348–353

[22] M. Baznat, K. Gudima, A. Sorin, O. Teryaev, Phys. Rev. C **88**, 061901 (2013) arXiv:1301.7003v1 [nucl-th]

[23] P. Huo, J. Jia, S. Mohapatra, Phys. Rev. C **90**, 024910 (2014)

[24] F. Becattini, F. Piccinini, and J. Rizzo, Phys. Rev. C **77**, 024906 – Published 21 February 2008

[25] H. Song, S.A. Bass, U. Heinz, T. Hirano, C. Shen, Phys. Rev. Lett. 106, 192301 – Published 9 May 2011; Erratum Phys. Rev. Lett. 109, 139904 (2012)

[26] L. P. Csernai, D. D. Strottman, Cs. Anderlik, Phys. Rev. C **85**, 054901

[27] D.J. Wang, Z. Néda, L.P. Csernai, Phys. Rev. C 87, 024908 (2013) arXiv:1302.1691v1 [nucl-th]

[28] L. P. Csernai, J. H. Inderhaug, Int. J. Mod. Phys. E 24, 1550013 (2015)

[29] G. Bunce *et al.*, Phys. Rev. Lett. 36, 1113

[30] G. L. Kane, J. Pumplin, W. Repko, Phys. Rev. Lett. 41, 1689

[31] P. Cea, P. Chiappetta, G. Nardulli, Physics Letters B, Volume 209, Issues 2–3, 1988, Pages 333–336

[32] B. L. Ioffe, D. E. Kharzeev, Phys. Rev. C 68, 061902(R), 2003

[33] ZT Liang, XN Wang Phys. Rev. Lett. 94, 102301 (2005); **Erratum***ibid.* 96, 039901 (2006)

[34] ZT Liang, J.Phys.G34:S323-330 (2007) arXiv:0705.2852v1 [nucl-th]

[35] V.P. Ladygin, A.P. Jerusalimov, N.B Ladygina, Phys. Part. Nucl. Lett. 7:349-354, 2010 arXiv:0806.3867v1

[36] A. Ipp, A. Di Piazza, J. Evers, C.H. Keitel, Physics Letters B, Volume 666, Issue 4, 4 September 2008, Pages 315–319

[37] STAR Collaboration: B.I. Abelev, I. Selyuzhenkov, *et al*, Phys. Rev. C **76**:024915,2007 arXiv:0705.1691v2 [nucl-ex]

[38] XG Huang, P. Huovinen, XN Wang, Phys. Rev. C **84**, 054910 (2011)

[39] JH Gao, SW Chen, WT Deng, ZT Liang, Q. Wang, XN Wang, Phys. Rev. C **77**, 044902 – Published 9 April 2008

[40] F. Becattini, V. Chandra, L. Del Zanna, E. Grossi, Annals Phys. 338 (2013) 32-49 arXiv:1303.3431v4 [nucl-th]

[41] G. Aad et al. (ATLAS Collaboration), Phys. Rev. D **91**, 032004 – Published 10 February 2015

[42] F. Becattini, L.P. Csernai, D.J. Wang, Phys. Rev. C **88**

[43] T. Csörgö, M. I. Nagy, Phys. Rev. C **89**, 044901 (2014) arXiv:1309.4390v3 [nucl-th]

[44] L.P. Csernai, S. Velle, International Journal of Modern Physics E Vol. 23, No. 9 (2014) 1450043, arXiv:1405.7283v2 [nucl-th]

[45] Yu.B. Ivanov, A.A. Soldatov, Phys. Rev. C **91**, 024915 (2015), arXiv:1412.1669v2 [nucl-th]

[46] Yu.B. Ivanov, A.A. Soldatov, Phys. Rev. C **91**, 024914 – Published 26 February 2015

[47] W. Zuo, SX Gan, U. Lombardo, Chinese Physics C 36 (2012) 967, arXiv:1310.1388v1 [nucl-th]

[48] E. Molnár, H. Niemi, D.H. Rischke, The European Physical Journal C, 65(3-4), 615-635 (2010)

[49] R.J. Glauber, Phys. Rev. 131, 2766 (1963)

[50] F. Gelis, Pramana Journal of physics, arXiv:1312.5497v2 [hep-ph]